The method of loop molecules and the topology of the Kovalevskaya top

A. V. Bolsinov and A. T. Fomenko

Department of Mechanics and Mathematics, Moscow State University
Moscow 119899, Russia

P. H. Richter

Institut für Theoretische Physik, Universität Bremen
28359 Bremen, Germany

October 22, 1999

Abstract

The topology of the Liouville foliation in the phase space of the Kovalevskaya top is completely characterized. It involves five distinct families of tori which are separated by 14 types of bifurcations. The bifurcations are organized by 13 different singularities, six of which are relative equilibria, and seven degenerate critical orbits. The bare molecules for the ten types of isoenergy surfaces have been determined earlier, but important information about the connection between admissible coordinate systems at different bifurcations has been missing so far. This gap is filled with the computation of marked molecules, based on a new method which uses molecules corresponding to loops around singular points in the bifurcation diagram. A global set of admissible coordinates is identified, and the molecules of all isoenergy surfaces are endowed with gluing matrices and topological marks.

Key words: Kovalevskaya top, Liouville foliation, bifurcation diagram, relative equilibria, degenerate critical orbits, topological atoms and molecules, admissible coordinate systems, gluing matrices

1 Introduction

The Kovalevskaya top is one of the most fascinating integrable systems in classical mechanics. Its discovery in 1889 by Sophia V. Kovalevskaya [19] was a highlight in the history of complex analysis, of which her teacher Karl Weierstrass was the leading figure of the time [8].

The system has the tantalizing property of not being separable in configuration space which, after reduction of the S^1-symmetry with respect to the axis of gravity, is the Poisson sphere. Nevertheless Kovalevskaya succeeded not only in finding a "fourth integral" in the six-dimensional phase space of Euler variables, the famous *Kovalevskaya integral* K which establishes integrability; she was also able to identify a set of phase space variables s_1, s_2, as coordinates on each Liouville torus, in terms of which the integration is reduced to an Abel-Jacobi inversion problem with a Riemann surface of genus 2. Hence it was demonstrated that the problem can be solved in terms of theta functions.

In a separate paper of the same year [20], Kovalevskaya proved that besides the cases of Euler, Lagrange, and her own, there is no other rigid body system that would be integrable, in terms of meromorphic functions of time, for any value of the angular momentum about the axis of gravity. This gives the three systems a highly prominent status among all rigid body systems. But while the Euler and Lagrange tops, because of their simplicity, have always been popular among physicists, the Kovalevskaya top has remained virtually unknown. In the classical book of Klein and Sommerfeld on spinning tops [17] it is mentioned only in passing. The reason, it seems, is its high degree of complexity. With the notable exception of Kötter's early analytic work [18], the system, until fairly recently, has almost exclusively been studied within the community of Russian mathematicians. For a review of the results obtained in the first one hundred years, see Bobenko et al. [3].

We recall only a few milestones of the development. The early work focused on analytical properties of the system. Zhukovsky [26] studied in detail the relationship of Kovalevskaya's variables (s_1, s_2) to the Euler variables $(p, q, r, \gamma_1, \gamma_2, \gamma_3)$. An important step for a comprehensive understanding was Appelrot's classification of critical orbits from an algebraic point of view [1]. The full nature of the bifurcation diagram, i. e., the set of critical values of the momentum mapping, was elucidated by Kharlamov in 1983 [15]. With this work, the attention shifted towards the topological structure of the system's phase space. It became one of the most challenging problems for the

classification theory of integrable Hamiltonian systems with two degrees of freedom that was developed by Fomenko et al. [13, 7, 23, 5] in the eighties. This work finally brought the Kovalevskaya system to the attention of physicists who were then able to calculate its actions and work out an action representation of its isoenergy surfaces [10, 11, 12].

The Kovalevskaya top is a system with three degrees of freedom, but due to the S^1-symmetry of the gravitational field it can be reduced to a one-parameter family of systems with two degrees of freedom. This is the generally adopted point of view for its description; the parameter l is the angular momentum with respect to the axis of gravity. It turns out that the momentum map $\mathcal{F}_l$ from phase space into the space of integrals H (energy) and K leads to ten topologically different types of isoenergy surfaces $(H, K) = \text{const}$ (assuming $l \geq 0$). The corresponding phase space foliations have been determined in terms of Fomenko "molecules" [23, 10]. However, for a globally complete topological characterization, one important set of data has been missing until now: the numerical marks (r, ε, n) on the edges of the molecules. These marks contain the relevant information on how the bifurcations at the vertices are related along the connecting edges.

This missing information is provided in the present paper. The topological analysis is thereby taken to completion. To achieve the goal, we have developed the *method of loop molecules* as a new tool in the topological theory. The key idea is to consider molecules corresponding to closed loops around singular points in the bifurcation diagram, and to identify admissible coordinate systems on the Liouville families of tori associated with the "atoms" of those molecules. The point is that these coordinate systems can all be given in terms of uniquely defined fundamental paths on the tori involved. Using the coordinate systems so defined for a comprehensive set of loop molecules, all bifurcations of the systems can be described with a globally defined set of paths. In the next step, we determine how the pattern of these paths is organized, and from there obtain the so-called "gluing matrices" for the molecules representing isoenergy surfaces. The gluing matrices, although not uniquely defined, contain all information about the marks (r, ε, n). The final results are given in Table 3.

This paper has three parts. In Section 2 we collect relevant concepts and facts from the topological theory of integrable Hamiltonian systems. The notation is taken from [5, 6]. Subsection 2.1 discusses singular points of bifurcation diagrams and how their loop molecules may be used, in general, to get global information about a system's topology. The following two subsections

provide lists of two kinds of loop molecules: those related to non-degenerate equilibria, and those associated with degenerate critical tori. In Section 3 we present the Kovalevskaya system: first its phase space structure and equations of motion (3.1), then various versions of its bifurcation diagram; in 3.2 we discuss a two-dimensional projection of the full three-dimensional bifurcation diagram, whereas in 3.3 the point of view of the reduced system with two degrees of freedom is assumed. The Appelrot classification of critical orbits is reviewed, and the two kinds of singular points (relative equilibria and degenerate critical orbits) are identified. In the last part, Section 4, the method of loop molecules is applied to the Kovalevskaya system. First the 13 loop molecules are determined in 4.1; next, in 4.2 we determine a global set of admissible coordinate systems for all bifurcations; then, in 4.3 we establish their global connections. The last subsection 4.4 finally drives in the harvest in terms of gluing matrices and the marked molecules of Table 3.

2 Topology of Liouville foliations

Consider an integrable Hamiltonian system on a symplectic manifold (M^4, ω) with Hamiltonian function H and an additional integral f. Let Σ be the bifurcation diagram of the momentum mapping $\mathcal{F} = (H, f) : M^4 \to \mathbf{R}^2$. The diagram Σ is located on the plane $\mathbf{R}^2(H, f)$. We assume Σ to be a collection of smooth curves $\gamma_1, \ldots, \gamma_k$ which may intersect or touch each other at certain points. In addition, we assume that the bifurcation of Liouville tori corresponding to each curve γ_j is non-degenerate, i. e., either of elliptic or hyperbolic type. In our terminology, it is represented by a certain "atom". Note that Σ may contain isolated points.

In this introductory section, we review some basic facts from the topological theory of phase space foliations and their representation in terms of molecules. Special emphasis is given to the set of singular points of the bifurcation diagram, and to the nature of corresponding loop molecules.

2.1 Singular points of bifurcation diagrams

Singular points of the bifurcation diagram Σ are points of intersection or of tangency, cusps, isolated points and so on; in other words: all points where Σ is not a smooth line.

Denote the set of singular points by Σ_0. We assume Σ_0 to be a finite set.

If we think of Σ as a one-dimensional cell complex, then Σ_0 is exactly the set of its vertices (zero-dimensional cells). The edges of the complex are the curves $\gamma_1, \ldots, \gamma_k$.

We say that a smooth curve τ without self-intersections lying in $\mathbf{R}^2(H,f)$ is *admissible* if it intersects Σ transversely and does not pass through singular points of Σ.

Its preimage $Q_\tau = \mathcal{F}^{-1}(\tau)$ in M^4 is a three-dimensional smooth manifold foliated into Liouville tori, and the singularities of this foliation are all non-degenerate. As a result, we can assign with Q_τ the so-called marked molecule which is a complete topological invariant of the Liouville foliation on Q_τ. We denote this molecule by $W^*(\tau)$. It is easy to see that $W^*(\tau)$ does not change under a smooth perturbation of τ in the class of admissible curves.

Now let $y_0 \in \Sigma_0$ be a singular point of the bifurcation diagram. Consider a circle τ of small radius centered at y_0. Assume that τ is admissible and that it remains so with decreasing radius. Then we can define the molecule $W^*(\tau)$.

Definition 1 *This molecule is said to be the* loop molecule *of the singular point $y_0 \in \Sigma$ and is denoted by $W^*(y_0)$.*

The idea to use loop molecules to describe the global topology of the Liouville foliation on isoenergy surfaces can be explained as follows. The loop molecule is a local invariant of a singularity. That is why it is usually more readily identified than the molecule for an isoenergy surface (which is a global invariant!). If the type of singularity related to a singular point $y_0 \in \Sigma_0$ is understood and described, then calculating the corresponding loop molecule is just a formal procedure and does not lead to any serious difficulties. Moreover, in specific problems we usually meet singularities from some finite list. One can collect such typical (standard) singularities and their loop molecules in advance, once and forever, and then use this list to study different systems.

Suppose we have already calculated the loop molecules for all singular points of a given bifurcation diagram. Then for any admissible curve $\tau \subset \mathbf{R}^2(H,f)$ the molecule $W^*(\tau)$ can be "glued" together from pieces of the loop molecules. It turns out that such a procedure makes it possible to get a lot of information about the desired molecule $W^*(\tau)$ (in particular, about its numerical marks). Sometimes one can completely calculate $W^*(\tau)$. Let us illustrate this idea by Figure 1. In Fig. 1(a) a bifurcation diagram with

three singular points y_1, y_2, y_3 is shown together with an admissible curve $\tau = \{H = h_0\}$. This curve intersects four smooth curves $\gamma_1, \gamma_2, \gamma_3, \gamma_4$ of Σ. Each of these curves corresponds to a certain bifurcation (i.e., atom) Q_i. The atoms Q_i are the same as those which occur in the loop molecules. So are the gluing matrices between atoms (it is better to say that the marks r and ε are the same, because the gluing matrices are not uniquely defined). For example, the molecules $W^*(\tau)$ and $W^*(y_1)$ have the common fragment Q_1—Q_2.

In Fig. 1(b) we show deformations of the "edges" of the loop molecules which drag these edges to the corresponding segments of the admissible curve τ. It is clear that under such deformations the topology does not change. As a result, the desired isoenergy molecule $W^*(\tau)$ (including information about gluing of Liouville tori) can be composed from the corresponding fragments of the loop molecules $W^*(y_1)$, $W^*(y_2)$ and $W^*(y_3)$.

A real situation may, of course, be more complicated. For example, it may happen that one segment of τ corresponds to several segments of different loop molecules (see Fig. 2). In this case we need some additional arguments to "compose" the gluing matrices for $W^*(\tau)$ from those of the loop molecules. We shall discuss such a procedure in Section 4.

A singular point of the bifurcation diagram may be the image under $\mathcal{F}$ of an equilibrium point $x \in M^4$, or it may be associated with a degenerate critical torus. We discuss these two possibilities in succession, and present lists of corresponding loop molecules.

2.2 Loop molecules of non-degenerate equilibria

Let us recall some properties of non-degenerate singularities of the momentum mapping. Consider an isolated equilibrium point $x \in M^4$ of an integrable Hamiltonian system (M^4, ω, H, f). Its image $y = \mathcal{F}(x)$ is obviously a singular point of the bifurcation diagram Σ. Non-degeneracy of x means that the eigenvalues of the linearized Hamiltonian system with Hamiltonian $H + cf$ (and some appropriate coefficient c) are all different and not zero. From the point of view of $\mathcal{F}$ the point x can be one of four different types, depending on these eigenvalues (λ and μ are assumed real and non-zero):

1. center–center: $\mathrm{i}\lambda$, $-\mathrm{i}\lambda$, $\mathrm{i}\mu$, $-\mathrm{i}\mu$;

2. center–saddle: $\mathrm{i}\lambda$, $-\mathrm{i}\lambda$, μ, $-\mu$;

3. saddle–saddle: λ, $-\lambda$, μ, $-\mu$;

4. focus–focus: $\lambda + \mathrm{i}\mu$, $\lambda - \mathrm{i}\mu$, $-\lambda + \mathrm{i}\mu$, $-\lambda - \mathrm{i}\mu$.

Remark 1. Instead of the initial Hamiltonian H we consider here a linear combination of H and f because for H itself some of the eigenvalues may coincide or be equal to zero, but this problem can be avoided by taking an appropriate linear combination. In other words, x may be degenerate for the Hamiltonian H, but non-degenerate for the momentum map $\mathcal{F} = (H, f)$.

Remark 2. Not all equilibrium points map to singular points of the bifurcation diagram. As an example, consider the combination of oscillator and rotator, $H(p_1, p_2, q_1, q_2) = p_1^2 + q_1^2 + p_2^2$, with $f = p_2$. The point is that such equilibria are not isolated; here, the coordinate q_2 can be chosen from a full circle. This circle is in fact a non-degenerate orbit generated by f (which, from the point of view of the foliation, ought to be considered as an independent Hamiltonian).

For these four types of non-degenerate singularities the loop molecules have been determined in [4, 22]. Among them, it is natural that our interest focuses on those which appear in specific problems of classical mechanics and mathematical physics. We have assembled a corresponding list based on the analysis of many examples of integrable systems which has recently been carried out in a series of papers [24, 16, 2, 9, 11, 23].

The result is presented in Table 1. For each loop molecule we mention integrable cases where the corresponding singularity appears. This list is, probably, not complete because we have not investigated all known integrable cases from this point of view.

2.3 Loop molecules of degenerate critical tori

Non-degenerate isolated periodic orbits come in two types, elliptic (stable) and hyperbolic (unstable). Their images under the momentum mapping trace out the regular part of the bifurcation diagram Σ. The singularities Σ_0 originate from degeneracies which occur when under changes of some parameter an orbit changes its type. In the examples that occur in classical mechanics, this means one of two scenarios: (i) transition from elliptic to hyperbolic or vice versa (pitchfork and period-doubling bifurcations); (ii) emergence or disappearance of criticality (saddle-node bifurcation). In all cases, the transition is characterized by the existence of a critical orbit with eigenvalue zero; such orbits are called parabolic.

We describe in the following the most frequently occuring singularities and give a list of the corresponding loop molecules, see Table 2.

Example 1: Saddle-node bifurcation.

Consider two functions $H = p_2$ and $f = f(p_1, q_1, p_2)$ in $\mathbf{R}^3(p_1, q_1, p_2)$ such that the level lines of f on surfaces $H = \text{const}$ have the form presented in Fig. 3, where the isoenergy surfaces appear as horizontal planes. It is seen that when the energy H increases, two non-degenerate critical points appear "out of nothing", one hyperbolic, the other elliptic. The functions H and f define a one-dimensional foliation in $\mathbf{R}^3$. Starting from there, one can naturally construct a two-dimensional foliation on $\mathbf{R}^3 \times S^1$ by taking the Cartesian product with a circle S^1. We let S^1 be parameterized with a periodic coordinate q_2 so that on $\mathbf{R}^3 \times S^1$ we have four coordinates p_1, q_1, p_2, q_2 which we define to be symplectic with 2-form $\omega = dp_1 \wedge dq_1 + dp_2 \wedge dq_2$. It is clear that $H(p, q)$ and $f(p, q)$ commute and define a Liouville foliation structure on the four-dimensional symplectic manifold $\mathbf{R}^3 \times S^1$. One can naturally consider $\mathbf{R}^3$ as a cross-section.

The corresponding bifurcation diagram Σ of the momentum mapping $\mathcal{F} : \mathbf{R}^3 \times S^1 \to \mathbf{R}^2(H, f)$ is also shown in Fig. 3. It has a cusp which is entirely located inside the image of $\mathcal{F}$. The singular point at the tip of the cusp has the loop molecule W_τ shown at the bottom right of Fig. 3.

To be explicit, f may be chosen as a function which in the neighborhood of the origin (the locus of the singularity) has the form

$$f = p_1^2 + q_1^3 - p_2 q_1. \tag{1}$$

This is exactly the canonical form of a hyperbolic singularity [14]. The set of critical points of $\mathcal{F}$ on the three-dimensional cross-section $\mathbf{R}^3$ is obtained from the requirement that the gradients of H and f be parallel; it is a parabola lying in the plane $p_1 = 0$ and given by $p_2 = 3q_1^2$. The singular points with $q_1 > 0$ are elliptic, those with $q_1 < 0$ are hyperbolic. For $q_1 = 0$ we have the parabolic singular point. The bifurcation diagram Σ on the plane $\mathbf{R}^2(H, f)$ is obtained by inserting $p_1 = 0$ and $q_1^2 = p_2/3 = H/3$ into the equation for f:

$$f = -2q_1^3 = \pm \frac{2}{3\sqrt{3}} H^{3/2}. \tag{2}$$

In case the system under consideration satisfies additional conditions, for example, if it admits a $\mathbf{Z}_2$-symmetry, two parabolic orbits may appear

simultaneously on the same leaf of the Liouville foliation. Such a case is illustrated in Fig. 4 where we also show the corresponding loop molecule.

Example 2: Elliptic pitchfork or period-doubling bifurcation.

The qualitative picture is again provided by two functions $H = p_2$ and $f = f(p_1, q_1, p_2)$ on $\mathbf{R}^3(p_1, q_1, p_2)$, with level lines of f on horizontal planes $H = \text{const}$ as shown in Fig. 5. When H increases, the elliptic singularity transforms into three non-degenerate singularities: two elliptic and one hyperbolic. The functions H and f define a one-dimensional foliation in $\mathbf{R}^3$ which can be transformed into a Liouville foliation on $\mathbf{R}^3 \times S^1$. But, unlike in the previous case, there are now two possibilities due to the $\mathbf{Z}_2$-symmetry.

The first possibility is to simply take the Cartesian product with the circle S^1. Let us call this the *orientable* case. As before, we take a 2π-periodic coordinate q_2 on S^1 and define the symplectic structure to be $\omega = dp_1 \wedge dq_1 + dp_2 \wedge dq_2$. It is clear that $H(p, q)$ and $f(p, q)$ commute and define a Liouville foliation on the symplectic 4-manifold $\mathbf{R}^3 \times S^1$. On a given isoenergy surface with sufficiently high H, there exist two different elliptic critical tori which are related by symmetry. The transition from one to three critical tori is a pitchfork bifurcation.

The second case, which we call *non-orientable*, can be described as follows. Multiply the foliation in $\mathbf{R}^3$ by the circle S^1 as before, but then take the quotient with respect to the $\mathbf{Z}_2$-action on $\mathbf{R}^3 \times S^1$ given by

$$(p_1, q_1, p_2, q_2) \mapsto (-p_1, -q_1, p_2, q_2 + \pi). \tag{3}$$

One can obtain the same result by multiplying the picture shown in Fig. 5 with the q_2-segment $[0, \pi]$ and gluing the ends $q_2 = 0$ and $q_2 = \pi$ of the cylinder so obtained, with a π-twist about the p_2 axis. This way of gluing implies that the two elliptic centers of a given high energy surface belong to one and the same critical torus. Thus the transition is from one to two critical tori; the continuation of the elliptic orbit turns hyperbolic while a new elliptic orbit of twice the period is born. This is a period-doubling bifurcation.

The bifurcation diagram of the momentum mapping $\mathcal{F} : \mathbf{R}^3 \times S^1 \to \mathbf{R}^2(H, f)$ is also shown in Fig. 5, together with the two loop molecules W_τ^{or} and W_τ^{nor} for the orientable and non-orientable cases, respectively.

A specific choice for f would be a function which locally has the form

$$f = p_1^2 + q_1^4 - p_2 q_1^2. \tag{4}$$

The set of critical points on the cross-section $\mathbf{R}^3$ has two parts:

$$\begin{aligned} &p_1 = 0, \quad q_1 = 0 \qquad \text{(a vertical line)}, \\ &p_1 = 0, \quad p_2 = 2q_1^2 \qquad \text{(a parabola in the vertical plane)}. \end{aligned} \tag{5}$$

The bifurcation diagram Σ in the (H, f)-plane consists of two pieces. The first one is the line $f = 0$. The second is the parabola arc $f = -H^2/2, H > 0$, see Fig. 5. Notice that the image of the momentum mapping is confined to the region $f \geq \min(0, -H^2/2)$; this is indicated by the shading in Fig. 5. The loop molecules have therefore no circular part.

Example 3: Hyperbolic pitchfork or period-doubling bifurcation.

This case is analogous to the previous one but with elliptic and hyperbolic singularities interchanged. The corresponding picture in $\mathbf{R}^3$ is presented in Fig. 6. One hyperbolic critical point transforms into one elliptic and two hyperbolic critical points. Again we distinguish two different extensions to a symplectic manifold $\mathbf{R}^3 \times S^1$: orientable and nonorientable. As before we put $H = p_2$ and, as a specific case, take f with the local behavior

$$f = p_1^2 - q_1^4 + p_2 q_1^2. \tag{6}$$

The set of critical points is the same as in (5). The bifurcation diagram is similar to the one of Example 2. Its two pieces are the straight line $f = 0$ and the parabola arc $f = H^2/2$, $H > 0$. Note, however, that here the entire neighborhood of the point $(H, f) = (0, 0)$ belongs to the image of the momentum map. This implies a different character for the loop molecules which now have a circular backbone, see Fig. 6.

Example 4: Modified hyperbolic pitchfork or period-doubling bifurcation.

This case is locally the same as the previous example. The set of critical points and the bifurcation diagram are identical. But the global picture is different: the separatrix is connected in another way, see Fig. 7. This implies that on the cross-section the atom D_1 is replaced by the atom C_2. The corresponding loop molecules are also shown in Fig. 7.

It is worth mentioning that in the non-orientable case we obtain the same molecule as in Example 3. The point is that the corresponding Liouville foliations are actually diffeomorphic (although this is not obvious).

Table 2 collects all loop molecules from Examples 1 through 4. We also mention a choice of well known integrable cases where these molecules occur.

The table is not complete; we confined ourselves to the most frequently occurring degenerate singularities. Among them we can distinguish the class of the so-called topologically stable singularities which preserve their topological structure under small integrable perturbations of the system. The classification from this point of view has recently been carried out by V. V. Kalashnikov Jr. [14]. In Table 2, the singularities 1, 4, 6 are stable; unstable singularities (2, 3, 7) usually occur due to some additional Z_2-symmetry which obstructs(???) their destruction.

3 The Kovalevskaya top

A general rigid body in a constant gravitational field, with one point fixed, has configuration space SO(3) and an S^1-symmetry, the φ-rotation about the direction of gravitation, called the *vertical* direction in the following. It is a system with three degrees of freedom, but after symmetry reduction one may view it as a two-degrees-of-freedom system, with the Poisson $\boldsymbol{\gamma}$-sphere as configuration space. It is convenient to embed this sphere into $\mathbf{R}^3(\boldsymbol{\gamma})$, and to choose the six-dimensional space $\mathbf{R}^6(\boldsymbol{\gamma}, \boldsymbol{l})$ as an appropriate phase space. $\boldsymbol{l} = (l_1, l_2, l_3)$ is the angular momentum and $\boldsymbol{\gamma} = (\gamma_1, \gamma_2, \gamma_3)$ a location on the vertical axes, both seen from a body-fixed reference system of principal axes. This phase space is endowed with the Poisson structure

$$\{\gamma_i, \gamma_j\} = 0, \qquad \{l_i, \gamma_j\} = \varepsilon_{ijk}\gamma_k, \qquad \{l_i, l_j\} = -\varepsilon_{ijk}l_k, \tag{7}$$

which may be written compactly in terms of the structure matrix

$$\mathbf{P} = \begin{pmatrix} \mathbf{0} & \hat{\boldsymbol{\gamma}} \\ -\hat{\boldsymbol{\gamma}} & \hat{\boldsymbol{l}} \end{pmatrix} \tag{8}$$

where $\hat{\boldsymbol{\gamma}}$ and $\hat{\boldsymbol{l}}$ are antisymmetric 3×3 matrices associated with $\boldsymbol{\gamma}$ and $\boldsymbol{l}$, respectively, $\hat{\gamma}_{ij} = -\varepsilon_{ijk}\gamma_k$ and $\hat{l}_{ij} = -\varepsilon_{ijk}l_k$. This structure possesses two Casimir constants,

$$C = \gamma_1^2 + \gamma_2^2 + \gamma_3^2 \qquad \text{geometric integral,} \tag{9}$$

$$L = \gamma_1 l_1 + \gamma_2 l_2 + \gamma_3 l_3 \qquad \text{angular momentum.} \tag{10}$$

Their constancy for any Hamiltonian motion, $\mathbf{P}\nabla C \equiv 0$ and $\mathbf{P}\nabla L \equiv 0$, reflects the fact that the system has effectively only two degrees of freedom.

The physical values of C and L are $C = 1$ (Poisson sphere) and $L = l$ (vertical component of the angular momentum). The manifold

$$M_l^4 = \{(\boldsymbol{\gamma}, \boldsymbol{l}) \in \mathbf{R}^6 : C = 1, L = l\} \tag{11}$$

is a natural symplectic manifold for rigid bodies with given angular momentum l. We call it the *reduced phase space*; compared to the full phase space $T^*SO(3)$ it ignores the φ-motion about the vertical axis in physical space. If that motion is of interest, it may be obtained from the motion in M_l^4 by integrating the equation

$$\dot{\varphi} = \frac{1}{\gamma_1^2 + \gamma_2^2}\Big(\frac{\gamma_1 l_1}{A_1} + \frac{\gamma_2 l_2}{A_2}\Big), \tag{12}$$

where A_i are the principal moments of inertia.

3.1 Equations of motion and integrals

The Kovalevskaya top has the special feature that its principal moments of inertia are $A_1 = A_2 = 2A_3 = 2$, and that the center of mass $\boldsymbol{c}$ is located on the symmetry plane of the ellipsoid of inertia. Without restricting the generality, we may assume $\boldsymbol{c} = (-1, 0, 0)$. The Hamiltonian is then

$$H = \frac{1}{4}(l_1^2 + l_2^2 + 2l_3^2) - \gamma_1. \tag{13}$$

The corresponding equations of motion are the Euler-Poisson-Kovalevskaya equations

$$\begin{pmatrix} \dot{\boldsymbol{\gamma}} \\ \dot{\boldsymbol{l}} \end{pmatrix} = \mathbf{P}\nabla H, \tag{14}$$

or explicitly,

$$\begin{pmatrix} \dot{\gamma}_1 \\ \dot{\gamma}_2 \\ \dot{\gamma}_3 \end{pmatrix} = \begin{pmatrix} \gamma_2 l_3 - \frac{1}{2}\gamma_3 l_2 \\ \frac{1}{2}\gamma_3 l_1 - \gamma_1 l_3 \\ \frac{1}{2}\gamma_1 l_2 - \frac{1}{2}\gamma_2 l_1 \end{pmatrix} \qquad \text{and} \qquad \begin{pmatrix} \dot{l}_1 \\ \dot{l}_2 \\ \dot{l}_3 \end{pmatrix} = \begin{pmatrix} \frac{1}{2} l_2 l_3 \\ -\frac{1}{2} l_3 l_1 - \gamma_3 \\ \gamma_2 \end{pmatrix}. \tag{15}$$

Besides the two Casimir constants and the energy integral $H = h$ this system admits an additional integral, the Kovalevskaya integral [19]

$$K = \left(\frac{l_1^2 - l_2^2}{4} + \gamma_1\right)^2 + \left(\frac{l_1 l_2}{2} + \gamma_2\right)^2. \tag{16}$$

It is straightforward to check $\{H, K\} = 0$. Hence, the system is integrable. The values of K will be denoted as k.

When the Kovalevskaya top is viewed as a system with three degrees of freedom, the phase space $\mathrm{T}^*\mathrm{SO}(3)$ is foliated by three-dimensional Liouville tori with labels (h, k, l). The momentum mapping

$$\mathcal{F} = (H, K, L) : \ \mathrm{T}^*\mathrm{SO}(3) \to \mathbf{R}^3(h, k, l) \tag{17}$$

possesses five three-dimensional ranges of regularity [15], separated by two-dimensional surfaces of the bifurcation diagram $\Sigma_{h,k,l}$ where the rank of the Jacobian $\mathrm{d}\mathcal{F}$ is less than 3. The system of surfaces of $\Sigma_{h,k,l}$ was organized into four classes by Appelrot's pioneering work [1]. It will be reviewed in subsection 3.3, but our emphasis is shifted from his primarily analytical distinction to a topological viewpoint. Within $\Sigma_{h,k,l}$ we may distinguish two special subsets: (i) a one-dimensional set $\Sigma^1_{h,k,l}$ of singular points, and (ii) the set $\Sigma^0_{h,k,l}$ of isolated points where two or more singular lines meet. This latter set consists of only seven points (h, k, l) which we call super-singular,

$$\Sigma^0_{h,k,l} = \{(2, 0, \pm 2), \left(\sqrt{3}, 0, \pm\tfrac{4}{3}\sqrt[4]{3}\right), \left(\tfrac{3}{2}, \tfrac{1}{4}, \pm\sqrt{2}\right), (0, 1, 0)\}. \tag{18}$$

The nature of these points will become clear in the following.

It is difficult to present the full three-dimensional bifurcation diagram $\Sigma_{h,k,l}$. Hence, several two-dimensional versions have been studied in the literature: the projection $\Sigma_{h,l}$ of $\Sigma^1_{h,k,l}$ onto $\mathbf{R}^2(h, l)$; the cross-section $\Sigma^l_{h,k} \subset \mathbf{R}^2(h, k)$ of $\Sigma_{h,k,l}$ at fixed l; the cross-section $\Sigma^h_{k,l} \subset \mathbf{R}^2(k, l)$ at fixed h. The first two versions are discussed in the following two subsections; for the third we refer to [25].

3.2 The bifurcation diagram $\Sigma_{h,l}$

The diagram $\Sigma_{h,l}$ was discussed in [23, 24, 10, 11, 25], see also [6]. It is shown schematically in Fig. 8; if it were drawn to scale, the cusps and regions I, J would hardly be visible. The lines of the diagram are projections of the singular set $\Sigma^1_{h,k,l}$ where rank $\mathrm{d}\mathcal{F} = 1$. We use two line styles to indicate different kinds of singular behavior. The fat lines are bifurcations in the topological character of the isoenergy surfaces, the thin lines are bifurcations of the Liouville foliation within a given topological type of isoenergy surface.

By isoenergy surfaces, we mean the three-dimensional subsets

$$Q^3_{h,l} = \{(\boldsymbol{\gamma}, \boldsymbol{l}) \in M^4_l : H = h\} \tag{19}$$

of the reduced phase space. Depending on (h, l), there exist four topological types of $Q^3_{h,l}$, not counting the empty set at $h < l^2/4 - 1$. As may be read off Fig. 8, they are S^3 at low energy or large angular momentum; $\mathbf{R}P^3$ at large h and small $|l|$; $S^2 \times S^1$ at large h and intermediate $|l|$; finally, K^3 in the tiny regions I near $(h, |l|) = (2, 2)$. The regions are formed by the fat lines of $\Sigma_{h,l}$ which are associated with relative equilibria of the reduced system, i. e., with solutions $(\boldsymbol{\gamma}, \boldsymbol{l}) = \text{const}$ of Eqs. (15):

H: sleeping top in hanging position, $\boldsymbol{\gamma} = (1, 0, 0)$, $\boldsymbol{l} = (l, 0, 0)$,

$$h = \frac{l^2}{4} - 1, \qquad k = (h + 2)^2; \tag{20}$$

U: sleeping top in upright position, $\boldsymbol{\gamma} = (-1, 0, 0)$, $\boldsymbol{l} = (-l, 0, 0)$,

$$h = \frac{l^2}{4} + 1, \qquad k = (h - 2)^2; \tag{21}$$

M: merry-go-round motion, with angular velocity $p = l_1/2$ as a parameter, $p^2 \leq 1$, and $\boldsymbol{\gamma} = (-p^2, 0, \sqrt{1 - p^4})$, $\boldsymbol{l} = (2p, 0, -\sqrt{1 - p^4}/p)$:

$$l = -p^3 - \frac{1}{p}, \qquad h = \frac{3}{2}p^2 + \frac{1}{2p^2}, \qquad k^2 = 0. \tag{22}$$

In the full system with three degrees of freedom, these relative equilibria exhibit only φ-motion, with constant velocity $\dot{\varphi}$ given by Eq. (12).

The lines of relative equilibria define two pairs of super-singular points from $\Sigma^0_{h,k,l}$:

S_1: the points of tangency of lines U and M,

$$(h, k, l) = (2, 0, \pm 2); \tag{23}$$

S_2: the cusps of lines M at

$$(h, k, l) = \left(\sqrt{3}, 0, \pm\tfrac{4}{3}\sqrt[4]{3}\,\right) \approx (1,7320, 0, \pm 3.0792). \tag{24}$$

The intersections of lines U and M at

$$(h, l) = \left(2\sqrt{2} - 1, \pm 2\sqrt{\sqrt{2} - 1}\right) \approx (1.8284, 3.3137). \tag{25}$$

are not associated with points from $\Sigma^0_{h,k,l}$ because the values of k are different on the two lines. From the picture of line M alone it is also not clear whether the cusp is a super-singular point; it might be an artifact of the projection. But in addition to the fat lines, there are thin lines which indicate degeneracies of critical orbits; the cusp is the point where line c, see below, branches off line M, hence it does belong to $\Sigma^0_{h,k,l}$.

Let us now discuss the three types of thin lines. They may be distinguished in terms of Appelrot's classification scheme [1, 11, 25]:

e: degeneracy of Appelrot class I, transition between classes II and III,

$$h = \tfrac{1}{2}l^2, \qquad k = 0; \tag{26}$$

c: degeneracy of Appelrot class IV,

$$h = \frac{3}{2}\Big(\frac{l^2}{2}\Big)^{1/3}, \qquad k = 1 - h^2/3, \qquad \big(l^2 \le \tfrac{16}{9}\sqrt{3}\big); \tag{27}$$

h: degeneracy of Appelrot class III, transition within class IV,

$$h = \frac{l^2}{2} + \frac{1}{l^2}, \qquad k = 1/l^4. \tag{28}$$

These lines define additional super-singular points from $\Sigma^0_{h,k,l}$:

S_3: the points of tangency of lines U, c, and h,

$$(h,k,l) = \big(\tfrac{3}{2}, \tfrac{1}{4}, \pm\sqrt{2}\big); \tag{29}$$

S_0: the point of tangency of lines c with the two signs of l,

$$(h,k,l) = (0,1,0). \tag{30}$$

The point S_1 is also an intersection with line e, and the cusp S_2 is the point where line c meets line M.

The system of lines in $\Sigma_{h,l}$ divides $\mathbf{R}^2(h,l)$ into 17 different regions with distinct types of Liouville foliation. If we identify regions which differ only in the sign of l, we are left with 10 different regions, denoted A, B, ..., J. (Notice that the line $l = 0$ is not singular, not even critical; hence the regions A, C, D appear only once in the full diagram.) The corresponding molecules have been identified in [15, 23, 10, 11, 2] and are by now well known, cf. Table 3. What has been missing until now is the structure of the gluing matrices for these molecules, or the numerical marks r, ε, n in the notation of [6, 7]. This is precisely the question to be settled in the present paper; the method of loop molecules is used to obtain the relevant information.

3.3 The bifurcation diagrams $\Sigma^l_{h,k}$

In the following we consider the Kovalevskaya top as a one-parameter family of systems with two degrees of freedom, with parameter l and phase spaces M^4_l. The Liouville tori for given (h, l) are two-dimensional in the three-dimensional isoenergy surface $Q^3_{h,l}$. The momentum mapping is

$$\mathcal{F}_l = (H, K) : \; M^4_l \to \mathbf{R}^2(h, k), \tag{31}$$

and the set of its critical values is the bifurcation diagram $\Sigma^l_{h,k}$. Clearly, this is the cross-section of $\Sigma_{h,k,l}$ at constant l.

With this point of view, the classification theory of Fomenko et al. [5, 6, 7] may be applied.

The bifurcation diagrams $\Sigma^l_{h,k}$ were first constructed by M. P. Kharlamov [15, 16], see also the work of A. A. Oshemkov [23, 24] and M. Audin [2]. Depending on the value of l, five cases must be distinguished:

a) $l = 0$.

b) $0 < |l| < \sqrt{2}$,

c) $\sqrt{2} < |l| < \frac{4}{3}\sqrt[4]{3}$,

d) $\frac{4}{3}\sqrt[4]{3} < |l| < 2$,

e) $|l| > 2$.

The corresponding bifurcation diagrams are shown in Fig. 9 a,b,c,d,e, with energy h drawn in the vertical and Kovalevskaya constant $k \geq 0$ in the horizontal direction. The various lines correspond to critical tori of Appelrot classes I through IV. The singular sets Σ^l_0 of these diagrams are cross-sections of the lines of $\Sigma^1_{h,k,l}$ with the planes $l = \text{const}$.

Let us first characterize the lines of critical tori, i. e., the Appelrot classes. In Fig. 9 they are identified by Appelrot's four numbers I through IV, and in Fig. 10 by a more refined nomenclature that involves altogether fourteen labels α_i, β_i, γ_i, δ_i. We assume $l \geq 0$.

Class I, also called Delone's class: the ray $k = 0$ in the energy range $h \geq \frac{l^2}{2}$; lines δ_1 and δ_2 in Fig. 10;

Class II: the parabola $k = (h - \frac{l^2}{2})^2$ in the range $\frac{l^2}{4} - 1 \leq h \leq \frac{l^2}{2}$; segments α_1 and α_2 in Fig. 10;

Class III: the same parabola $k = (h - \frac{l^2}{2})^2$ in the range $\frac{l^2}{2} \le h \le \frac{l^2}{2} + \frac{1}{l^2}$; segments β_1, β_2, β_3 in Fig. 10;

Class IV: the curve given parametrically by $k = 1 + lp + p^4$ and $h = p^2 - l/2p$; the piece with positive $p \ge l/2$ is line γ_1 in Fig. 10, various pieces with p from $(-\infty, 0)$ are γ_2 through γ_7.

The point H at the bottom of each diagram is $(h, k) = \left(\frac{l^2}{4} - 1, (\frac{l^2}{4} + 1)^2\right)$. It is the sleeping top in hanging position. The left boundary consists of the lines of classes I and II, while the right boundary $k_{\max}$ is given by line γ_1 of class IV. Classes III and IV (except for γ_1) define interior lines.

Using the established notation for non-degenerate bifurcations [5, 6], we indicate in Fig. 9 what type of transition occurs at any given line. The Kovalevskaya system involves the four types

$$A, A^*, B, C_2 \tag{32}$$

whose topological nature is exhibited in Fig. 11. The following list collects the information that has accumulated in the literature:

line	*bifurcation type*	*line*	*bifurcation type*
δ_1	$A + A$	γ_1	A
δ_2	$A + A$	γ_2	$A^* + A^*$
α_1	A	γ_3	B
α_2	$A + A$	γ_4	A
β_1	B	γ_5	B
β_2	C_2	γ_6	$B + B$
β_3	$B + B$	γ_7	$A + A$

(33)

Using this knowledge, it is straightforward to construct the molecules $W^*(\tau)$ for paths τ in $\mathbf{R}^2(h, k)$. In particular, the molecules for fixed values of (h, l) and varying k, associated with points of the diagram $\Sigma_{h,l}$, can be assembled for all 10 types of foliation: simply follow the horizontal lines with labels A through J in Fig. 9, and keep track of the intersections with curves γ_i. Table 3 contains the complete list.

The lines of critical values divide the image of the momentum mapping into a number of regions of regularity where the families of existing Liouville tori do not undergo bifurcations. In the full bifurcation diagram

$\Sigma_{h,k,l}$ the lines from $\Sigma^l_{h,k}$ are drawn out into the l-direction and form two-dimensional surfaces; these surfaces define five different regions (i) through (v) in $\mathbf{R}^3(h,k,l)$ called Kharlamov regions in [11]. But note that the preimage of a given point (h,k,l) may consist of several Liouville tori, some related by symmetries, others not. From our topological viewpoint we prefer to think of families of Liouville tori rather than of their images under $\mathcal{F}$. It turns out that up to symmetry, there are again five distinct families of Liouville tori which we denote by (1), (2), (3), (4), (5). Several families of tori may map to the same Kharlamov region under $\mathcal{F}$. The exact scheme is as follows:

Liouville families		*Kharlamov region*
(1)	$\mapsto$	(i)
two (2)	$\mapsto$	(ii)
two (3)	$\mapsto$	(iii)
(1) and (4)	$\mapsto$	(iv)
two (2) and two (5)	$\mapsto$	(v)

(34)

The cross-sections of the Kharlamov regions at constant l are seen in $\Sigma^l_{h,k}$, and we indicate in Fig. 10 which families of Liouville tori are mapped into them.

To understand the relation between the bifurcation diagrams $\Sigma^l_{h,k}$ and bifurcations in families of Liouville tori, consider Fig. 10 b and the critical curves γ_3, γ_4. When a point (h,k) crosses γ_4 coming from high values of k, nothing happens to the family (1). The bifurcation A mentioned in Fig. 9 b only affects family (4) which is born in this transition. Upon further reducing k, the tori of families (1) and (4) combine in a bifurcation of type B on line γ_3.

On the other hand, notice that in Fig. 10 some curves are given two names: γ_1, γ_4 in Fig. 10 a and δ_1, δ_2 in Figs. 10 d,e. The reason is that two different families of tori undergo bifurcations when the same line in $\mathbf{R}^2(h,k)$ is crossed.

Each bifurcation diagram $\Sigma^l_{h,k}$ has a set Σ^l_0 of singular points. In Fig. 9 they are seen as intersections or tangencies of lines, or as the cusp if $l < \frac{4}{3}\sqrt[4]{3}$. These singular sets establish the correspondence with the diagram $\Sigma_{h,l}$ in Fig. 8 which is obtained by following the singular points in Figs. 9 as the angular momentum l varies, and plotting their energy h versus l. The fat points H, U_1, U_2, U_3, M_1, M_2 in Figs. 9/10 are parameter values of relative

equilibria and trace out the fat lines H, U, M in Fig. 8, respectively. Their topological character is specified in the following table [4, 21]:

point	*type*	*topological structure*
H	center-center	$A \times A$
U_1	saddle-saddle	$(B \times C_2)/\mathbf{Z}_2$
U_2	saddle-saddle	$B \times B$
U_3	center-saddle	$A \times B$
M_1	center-center	$2(A \times A)$
M_2	center-saddle	$A \times B$

(35)

There are no singularities of focus-focus type in the Kovalevskaya system.

The other singular points correspond to degenerate closed trajectories of various types, and when l is varied, they form the lines e, c, h in the diagram $\Sigma_{h,k,l}$: line e derives from the point where classes I, II, and III join; line c comes from the cusp at $p = -(l/4)^{1/3}$ on line IV; line (h) is obtained from the points where line III ends and touches line IV ($p = -1/l$). But depending on the range of l, the neighborhood of these points is different so that for each of them we have to distinguish two kinds. The following list collects what is known about their character:

singular point	*range of* l	*type of degeneracy*
S_0	$l = 0$	elliptic pitchfork
e_1	$0 < \lvert l\rvert < 2$	elliptic pitchfork
e_2	$\lvert l\rvert > 2$	elliptic pitchfork
c_1	$0 < \lvert l\rvert < \sqrt{2}$	saddle-node
c_2	$\sqrt{2} < \lvert l\rvert < \frac{4}{3}\sqrt[4]{3}$	saddle-node
h_1	$0 < \lvert l\rvert < \sqrt{2}$	hyperbolic pitch-fork
h_2	$\lvert l\rvert > \sqrt{2}$	hyperbolic period-doubling

(36)

There is no elliptic period-doubling in the Kovalevskaya system.

4 Analysis and application of loop molecules

The aim of this section is to calculate the marks (r, ε, n) on the molecules in Table 3. They determine unambiguously how the coordinate systems on

Liouville tori of a family change as we move along an edge, from one of its vertices to the other.

To compute these marks, we develop here the new method of loop molecules. It consists of four steps. First we collect a table of loop molecules for all singular points. Then we use them to construct, at each singular point, a set of admissible coordinate systems which only involves uniquely defined cycles; a subset of these admissible coordinate systems is selected for global purposes in such a way that only one such system is used everywhere along a given bifurcation. In the third step, we analyze how the various admissible coordinate systems defined for a given family are related on the fundamental lattices of their tori. This knowledge enables us to do the last step and determine the gluing matrices which connect the admissible coordinate systems of neighboring atoms along the edge of a molecule; the marks follow as a byproduct.

The main result can be formulated as

Theorem 1 *The complete list of marked molecules for the isoenergy surfaces in the Kovalevskaya system consists of the 10 cases presented in Table 3.*

The rest of this section is the proof of this theorem.

In the more general parts where we explain the method independently of the Kovalevskaya system, we denote, as in Section 2, edges of the bifurcation diagram $\Sigma^l(h,k)$ as γ_i, and vertices as y_0.

4.1 The list of loop molecules

Using our knowledge about the character of the various Appelrot lines α_i, β_i, γ_i, δ_i, we can assemble the loop molecules $W^*(y_0)$ for all 13 different singular points y_0. This is done in Table 4. The notation is explained with the following example:

$$\begin{array}{c} {\scriptstyle (1)}\searrow \\ \\ {\scriptstyle (5)}\nearrow \end{array} \quad B_{\boxed{\gamma_6}} \quad \xrightarrow{(2)} \tag{37}$$

The essence of this structure is the atom $>B-$. The direction of the arrows indicates increasing k. The numbers (n) on the arrows denote the family of Liouville tori corresponding to the respective edge. The index $\boxed{\gamma_6}$ tells on which Appelrot line the bifurcation B occurs.

The remaining information in Table 4 are the marks r. For an edge connecting bifurcations i and j the mark r indicates how the uniquely defined cycles λ_i and λ_j of the two atoms (see the following subsection) intersect when they are considered on the same torus. According to the code defined in [4], λ_i and λ_j have intersection index

0 if $r = \infty$ (the cycles are then homologous),

1 if $r = 0$,

2 if $r = \frac{1}{2}$.

The determination of r is not difficult if the type of singularity of y_0 is known, see Figs. 4 to 7 and 11.

4.2 Admissible coordinates on Liouville tori

Consider the preimage under $\mathcal{F}_l$ of a smooth segment τ that intersects an edge $\gamma_i \subset \Sigma^l_{h,k}$ transversely. Topologically this is a three-dimensional manifold Q_i whose boundary ∂Q_i is a collection of Liouville tori; we call it a *3-atom*. On each of these boundary tori we can define a pair of basic cycles (λ, μ) in such a way that they form an *admissible coordinate system* on ∂Q_i in the sense defined in [6, 7]. For the atoms A, A^*, B, C_2 which occur in the Kovalevskaya system, they are shown in Fig. 11. For atom A the manifold Q is a full torus with the elliptic orbit as its central fiber. For atom B we have a full torus surrounding the hyperbolic orbit, but with two smaller full tori taken out of its interior. The two hollow tori are not entangled with each other nor with the hyperbolic orbit. In case of atom A^* the manifold Q is again a full torus aligned with the hyperbolic orbit, and a single full torus with winding number 2 is taken out of its interior. Finally, atom C_2 corresponds to a full torus minus three inner full tori, all three of them with winding number 1 and without mutual entanglement.

The important fact is that for a given torus within Q, the first basic cycle λ is always uniquely defined and continuous at the transition. In the bifurcations B, A^*, C_2 of hyperbolic type, λ is just the unstable periodic orbit moved to the given torus (any of the two hyperbolic orbits will do in case C_2 because they are homotopic within Q). If the bifurcation is of type A, then λ is the cycle which shrinks to a point on the elliptic orbit. In contrast, the second cycle μ varies discontinuously in all four cases, and is not uniquely

defined. For example, in case A, a given μ may have any number of λ added to it; in case A^*, see Fig. 11c, any number of $\lambda/2$ may be added to μ.

In the following we denote by λ_i the first basic cycle on the atom Q_i; in specific cases of the Kovalevskaya system, i will be replaced by one of the 14 symbols $\delta_1, ..., \gamma_7$ from (33). A transition of type A is symbolically represented as

$$A_{\boxed{i}} \xrightarrow{(n)} (\lambda_i, \mu_i^+) \qquad \text{or} \qquad (\lambda_i, \mu_i^-) \xrightarrow{(n)} A_{\boxed{i}} \tag{38}$$

depending on whether the family (n) appears or disappears with increasing k. A transition of type B might look like

$$\begin{matrix} (\lambda_i, \mu_{im}^-) & \overset{(m)}{\searrow} \\ & B_{\boxed{i}} \xrightarrow{(n)} (\lambda_i, \mu_{in}^+); \\ (\lambda_i, \mu_{in}^-) & \underset{(n)}{\nearrow} \end{matrix} \tag{39}$$

tori from families (m) and (n) merge to form a single family (n). Their cycles λ_i are the same, but the cycles μ_{im}^- and μ_{in}^- below the transition, and μ_{in}^+ above the transition, are not continuously related. (It often happens, however, that a sum rule of the kind $\mu_{im}^- + \mu_{in}^- = \mu_{in}^+$ applies at the transition.)

To proceed with the analysis, we have to choose admissible coordinate systems for each bifurcation γ_i. This will endow each family involved in the bifurcation with a pair of cycles (λ_i, μ_i). Now remember that the λ_i do not change in a bifurcation of hyperbolic type (they disappear, together with the family, at elliptic bifurcations A), hence they are the same in all participating families. As to the μ_i, they are chosen is such a way that they all lie in an appropriate cross section of the atom under consideration.

When a given Liouville family undergoes different bifurcations γ_i and γ_j, this procedure generates, in general, different pairs (λ_i, μ_i) and (λ_j, μ_j) from the fundamental group of the family's tori. But when we analyze the loop molecule for a given singular point, then for the bifurcations connecting to that point, the μ_i can be chosen to be identical with certain λ_j defined by other bifurcations. In this way each loop molecule can be constructed with admissible coordinate systems which are made up entirely of cycles λ_i. Let us explain this with an example.

Consider the point U_2 which according to (35) is a relative equilibrium of saddle-saddle type and can be represented as the direct product $B \times B$ of the two simplest saddle bifurcations, see Fig. 12. For the time being, we

denote the cycles on the boundaries of the two fat figures eight P and P' by α, β, γ, and α', β', γ', as indicated in the figure.

The point U_2 is connected to the four non-degenerate bifurcations β_1, β_3, γ_5, γ_6. We must now determine how the atoms corresponding to these bifurcations are related to the direct product $P \times P'$.

Q_{β_1} is obtained by taking the direct product of the exterior boundary cycle α of P with the entire fat figure eight P';

Q_{β_3} is obtained by taking the direct product of the two interior boundary cycles β and γ of P with the entire fat figure eight P';

Q_{γ_5} is obtained by taking the direct product of the exterior boundary cycle α' of P' with the entire fat figure eight P;

Q_{γ_6} is obtained by taking the direct product of the two interior boundary cycles β' and γ' of P' with the entire fat figure eight P.

In fact, this description can be taken as a characterization of singularities of type $B \times B$. To construct the corresponding loop molecule, consider the admissible coordinate systems involved. The atom Q_{β_1} has three boundary tori, see Fig. 12; the basic cycles on them can be taken as $(\alpha, -\alpha')$, (α, β'), and (α, γ'). (The minus sign is needed to get the correct orientations, see below.)

For the other three atoms, admissible coordinate systems are constructed in the same way. Now notice that the cycle α is nothing but λ_{β_1}, the first basic cycle of atom Q_{β_1}. Similarly, α' is λ_{γ_5}, both β and γ are λ_{β_3}, and β' as well as γ' are λ_{γ_6}. As a result, we obtain the following set of admissible

coordinate systems for the bifurcations involved with the singular point U_2:

$$
\begin{array}{lllll}
Q_{\beta_1}: & \begin{array}{l}(\lambda_{\beta_1}, \quad \lambda_{\gamma_6}) \\ (\lambda_{\beta_1}, \quad \lambda_{\gamma_6})\end{array} & \begin{array}{l}\overset{(2)}{\searrow} \\ \overset{(2)}{\nearrow}\end{array} & B\boxed{\beta_1} & \overset{(1)}{\longrightarrow} \quad (\lambda_{\beta_1}, -\lambda_{\gamma_5}) \\
Q_{\beta_3}: & \begin{array}{l}(\lambda_{\beta_3}, \quad \lambda_{\gamma_6}) \\ (\lambda_{\beta_3}, \quad \lambda_{\gamma_6})\end{array} & \begin{array}{l}\overset{(2)}{\searrow} \\ \overset{(5)}{\nearrow}\end{array} & B\boxed{\beta_3} & \overset{(3)}{\longrightarrow} \quad (\lambda_{\beta_3}, -\lambda_{\gamma_5}) \\
Q_{\gamma_5}: & \begin{array}{l}(\lambda_{\gamma_5}, -\lambda_{\beta_3}) \\ (\lambda_{\gamma_5}, -\lambda_{\beta_3})\end{array} & \begin{array}{l}\overset{(3)}{\searrow} \\ \overset{(3)}{\nearrow}\end{array} & B\boxed{\gamma_5} & \overset{(1)}{\longrightarrow} \quad (\lambda_{\gamma_5}, \quad \lambda_{\beta_1}) \\
Q_{\gamma_6}: & \begin{array}{l}(\lambda_{\gamma_6}, -\lambda_{\beta_3}) \\ (\lambda_{\gamma_6}, -\lambda_{\beta_3})\end{array} & \begin{array}{l}\overset{(2)}{\searrow} \\ \overset{(5)}{\nearrow}\end{array} & B\boxed{\gamma_6} & \overset{(2)}{\longrightarrow} \quad (\lambda_{\gamma_6}, \quad \lambda_{\beta_1})
\end{array}
\tag{40}
$$

The other singular points can be analyzed in much the same way. As a second example, we present the result for the singular point U_1 which is slightly more complicated because its type is not a simple direct product but $(B \times C_2)/\mathbf{Z}_2$, see (35):

$$
\begin{array}{lllll}
Q_{\beta_1}: & \begin{array}{l}\left(\lambda_{\beta_1}, -\frac{\lambda_{\beta_1}+\lambda_{\gamma_2}}{2}\right) \\ \left(\lambda_{\beta_1}, -\frac{\lambda_{\beta_1}+\lambda_{\gamma_2}}{2}\right)\end{array} & \begin{array}{l}\overset{(2)}{\searrow} \\ \overset{(2)}{\nearrow}\end{array} & B\boxed{\beta_1} & \overset{(1)}{\longrightarrow} \quad (\lambda_{\beta_1}, \lambda_{\beta_1} + \lambda_{\gamma_3}) \\
Q_{\beta_2}: & \begin{array}{l}(\lambda_{\beta_2}, -\lambda_{\gamma_2}) \\ (\lambda_{\beta_2}, -\lambda_{\gamma_2})\end{array} & \begin{array}{l}\overset{(3)}{\searrow} \\ \overset{(3)}{\nearrow}\end{array} & C_2\boxed{\beta_2} & \begin{array}{ll}\overset{(1)}{\nearrow} & (\lambda_{\beta_2}, \quad \lambda_{\gamma_3}) \\ \overset{(4)}{\searrow} & (\lambda_{\beta_2}, \quad \lambda_{\gamma_3})\end{array} \\
Q_{\gamma_2}: & \left(\lambda_{\gamma_2}, \quad \frac{\lambda_{\beta_1}+\lambda_{\gamma_2}}{2}\right) & \overset{(2)}{\longrightarrow} & A^*\boxed{\gamma_2} & \overset{(3)}{\longrightarrow} \quad (\lambda_{\gamma_2}, -\lambda_{\beta_2}) \\
Q_{\gamma_3}: & (\lambda_{\gamma_3}, \quad \lambda_{\beta_1}) & \overset{(1)}{\longrightarrow} & B\boxed{\gamma_3} & \begin{array}{ll}\overset{(1)}{\nearrow} & (\lambda_{\gamma_3}, -\lambda_{\beta_2}) \\ \overset{(4)}{\searrow} & (\lambda_{\gamma_3}, -\lambda_{\beta_2})\end{array}
\end{array}
\tag{41}
$$

Notice that the two schemes (40) and (41) give two different admissible coordinate systems for the atom Q_{β_1}. This comes as no surprise because, as was already explained, admissible coordinate systems are not uniquely defined.

However, a choice has to be made here. The final goal of the present analysis is to identify a global set of gluing matrices, or marks, for the loop

molecules of all singular points; global in the sense that when the paths τ surrounding one singularity are dragged into the neighborhood of another singularity, as described in Fig. 2, the same coordinate systems are used. In other words, in what follows we take the same admissible coordinate system all along a given bifurcation i. If we decide, as we will, to use for β_1 the system that comes from (40), we must determine how the cycle $(\lambda_{\beta_1} + \lambda_{\gamma_2})/2$ can be expressed in terms of λ_{β_1} and λ_{γ_6}, and λ_{γ_3} in terms of λ_{β_1} and λ_{γ_5}. This will be done in the next subsection.

To obtain complete information on the loop molecules of Table 4, all 13 singular points H, $\mathrm{U}_{1,2,3}$, $\mathrm{M}_{1,2}$, S_0, $\mathrm{e}_{1,2}$, $\mathrm{c}_{1,2}$, $\mathrm{h}_{1,2}$ must be subject to the analysis that we presented in (40) and (41) for the examples U_2 and U_1 respectively. The simplest case is point H which gives the following picture for the two elliptic bifurcations α_1 and γ_1:

$$\begin{array}{lcl} Q_{\alpha_1}: & A_{\boxed{\alpha_1}} & \xrightarrow{(1)} \quad (\lambda_{\alpha_1}, \lambda_{\gamma_1}) \\ Q_{\gamma_1}: & (\lambda_{\gamma_1}, \lambda_{\alpha_1}) & \xrightarrow{(1)} \quad A_{\boxed{\gamma_1}} \end{array} \tag{42}$$

Inspecting Fig. 11 a we see that the intersection number of cycles (λ_{α_1} and λ_{γ_1}) must be 1, hence $r = 0$ for $W^*(\mathrm{H})$.

Other admissible coordinate systems for the bifurcation α_1 come from consideration of points $\mathrm{e}_{1,2}$, U_3, and for γ_1 we get another admissible coordinate system from point S_0. Again we have to make a choice which system we want to use for the global analysis.

In principal, we might start at any singular point such as H, and proceed from there along the various bifurcation lines to investigate the other singular points one by one. The set of gluing matrices that we finally get – not the marks! – depends on the choice of our starting point. It turns out that the best strategy, in terms of overall simplicity, is to start from a singular point somewhere in the center of the bifurcation diagram. We choose this point to be U_2.

From the neighborhoods of points U_2 and U_1 we have so far constructed admissible coordinate systems for the atoms related to the seven hyperbolic bifurcations β_1, β_2, β_3, γ_2, γ_3, γ_5, γ_6. The remaining bifurcations are of elliptic type, i. e., they involve atoms of type A, see (33). We define the admissible coordinate systems for Q_{γ_1} and Q_{γ_4} by looking at the loop molecule for S_0; for Q_{α_1} and Q_{δ_1} we take the singular point e_1, and e_2 for Q_{α_2} and Q_{δ_2}. All these singularities are elliptic pitchforks, see (36). Therefore, as can be seen

from Fig. 5, the second basic cycle μ can be chosen as the "axis" of the neighboring atom B. Finally, an admissible coordinate system for the atom Q_{γ_7} is obtained with the singular point h_2 which is of hyperbolic period-doubling type. Its second cycle μ is taken as $(\lambda + \lambda')/2$, where λ' is the "axis" of the neighboring B:

$$\begin{array}{lcl}
Q_{\gamma_1}: & (\lambda_{\gamma_1}, \lambda_{\gamma_3}) & \xrightarrow{(1)} \quad A_{\boxed{\gamma_1}} \\
Q_{\gamma_4}: & (\lambda_{\gamma_4}, \lambda_{\gamma_3}) & \xrightarrow{(4)} \quad A_{\boxed{\gamma_4}} \\
Q_{\alpha_1}: & A_{\boxed{\alpha_1}} & \xrightarrow{(1)} \quad (\lambda_{\alpha_1}, \lambda_{\beta_1}) \\
Q_{\delta_1}: & A_{\boxed{\delta_1}} & \xrightarrow{(2)} \quad (\lambda_{\delta_1}, \lambda_{\beta_1}) \\
Q_{\alpha_2}: & A_{\boxed{\alpha_2}} & \xrightarrow{(3)} \quad (\lambda_{\alpha_2}, \lambda_{\beta_3}) \\
Q_{\delta_2}: & A_{\boxed{\delta_2}} & \xrightarrow{(5)} \quad (\lambda_{\delta_2}, \lambda_{\beta_3}) \\
Q_{\gamma_7}: & A_{\boxed{\gamma_7}} & \xrightarrow{(5)} \quad \left(\lambda_{\gamma_7}, \frac{\lambda_{\gamma_7}+\lambda_{\beta_3}}{2}\right)
\end{array} \tag{43}$$

Let us summarize what we have achieved in this subsection. For each of the 13 singular points, we have constructed admissible coordinate systems for the associated atoms: explicitly for H in (42), U_1 in (41), U_2 in (40), and implicitly for the ten remaining loop molecules listed in Table 4. For a given bifurcation, this process generates, in general, several different systems. In order to get a coherent global description of the topology, we have then selected one particular admissible coordinate system for each of the 14 bifurcations. With this information, we are now in the position to determine a global set of gluing matrices, or marks (r, ε, n).

4.3 Relation between basic cycles on Liouville tori

Let us explain with an example how we determine the gluing matrix for the edge of a molecule. At low energies h, the isoenergy surface is represented by the simplest possible molecule $W^*(\mathrm{H})$,

$$A_{\boxed{\alpha_1}} \quad \xrightarrow{(1)} \quad A_{\boxed{\gamma_1}}, \tag{44}$$

denoted as type A in [11]. From (42) we have the admissible coordinate systems $(\lambda_{\alpha_1}, \lambda_{\gamma_1})$ and $(\lambda_{\gamma_1}, \lambda_{\alpha_1})$ for the two atoms. The transition matrix $\mathbf{C}$

between the two sets is obviously

$$\begin{pmatrix}\lambda_{\gamma_1}\\ \lambda_{\alpha_1}\end{pmatrix} = \mathbf{C}\begin{pmatrix}\lambda_{\alpha_1}\\ \lambda_{\gamma_1}\end{pmatrix} = \begin{pmatrix}0 & 1\\ 1 & 0\end{pmatrix}\begin{pmatrix}\lambda_{\alpha_1}\\ \lambda_{\gamma_1}\end{pmatrix}. \tag{45}$$

However, this is not the matrix given in Table 5. The reason is that it does not use the basis that we decided in (43) to use for global purposes. The admissible coordinate systems for α_1 and γ_1 ought to be $(\lambda_{\alpha_1}, \lambda_{\beta_1})$ and $(\lambda_{\gamma_1}, \lambda_{\gamma_3})$, respectively. Hence the matrix $\mathbf{C}$ that we look for is defined by

$$\begin{pmatrix}\lambda_{\gamma_1}\\ \lambda_{\gamma_3}\end{pmatrix} = \mathbf{C}\begin{pmatrix}\lambda_{\alpha_1}\\ \lambda_{\beta_1}\end{pmatrix}. \tag{46}$$

In order to find it explicitly, notice that $(\lambda_{\alpha_1}, \lambda_{\beta_1})$ and $(\lambda_{\gamma_1}, \lambda_{\gamma_3})$ are two different bases in the same family (1) of Liouville tori; all we need to know is how these bases are related. Fig. 13 a tells us that $\lambda_{\gamma_1} = -2\lambda_{\alpha_1} + \lambda_{\beta_1}$ and $\lambda_{\gamma_3} = -\lambda_{\alpha_1} + \lambda_{\beta_1}$. This gives the gluing matrix

$$\mathbf{C} = \begin{pmatrix}-2 & 1\\ -1 & 1\end{pmatrix}. \tag{47}$$

But how do we get the information given in Fig. 13? We extract it from the marks r on the loop molecules in Table 4. Consider as an example the loop molecule e_1. Table 4 tells us that the cycles λ_{α_1} and λ_{β_1} have intersection index 1 in family (1), and that λ_{β_1}, λ_{δ_1} have intersection index 1 in family (2). That this is so follows from the fact that e_1 is an elliptic pitchfork singularity of orientable type, see Fig. 5 and also Fig. 11 a,b.

Let us now analyze each family separately.

Family (1). This family participates in the bifurcations $A_{\boxed{\gamma_1}}$, $A_{\boxed{\alpha_1}}$, $B_{\boxed{\beta_1}}$, $C_2{}_{\boxed{\beta_2}}$, $B_{\boxed{\gamma_3}}$, $B_{\boxed{\gamma_5}}$. The singular points involved are are H, U_1, U_2, U_3, S_0, e_1, h_1. The information that can be extracted from the corresponding loop molecules is as follows.

H: λ_{γ_1} and λ_{α_1} have intersection index 1.

U_1: λ_{β_2} and λ_{γ_3} as well as λ_{β_1} and λ_{γ_3} have intersection index 1.

U_2: λ_{β_1} and λ_{γ_5} have intersection index 1.

U_3: λ_{α_1} and λ_{γ_5} have intersection index 0, i.e., are homologous up to a sign.

S_0: λ_{γ_1} and λ_{γ_3} have intersection index 1.

e_1: λ_{α_1} and λ_{β_1} have intersection index 1.

h_1: λ_{β_2} and λ_{γ_5} have intersection index 0, i.e., are homologous.

Now remember that all six cycles λ_i mentioned in the above listing belong to the integer lattice Γ of fundamental cycles on a torus $T \in (1)$. We may consider $(\lambda_{\gamma_1}, \lambda_{\alpha_1})$ as a basis of that lattice. To obtain the arrangement of Fig. 13 a for the other four cycles, we use the above statements on intersection indices together with the following convention on orientations.

Two admissible coordinate systems (λ_i, μ_i) and (λ_j, μ_j) on opposite sides of the edge connecting atoms i and j are called *compatible* in terms of orientation, if the transition matrix $\mathbf{C}$ between them has determinant -1 (in other words, the orientations are opposite). This rule can be reformulated by saying that if the two bifurcations i and j are both located on the left side of region (1) in Fig. 10, then the orientations of the corresponding admissible coordinate systems coincide, otherwise they are opposite. Furthermore, a subtle argument involving symmetry is helpful in our considerations. Consider first the bifurcation $A_{\boxed{\gamma_4}}$ as it affects Family (4). Depending on whether we discuss it with the singular points c_1 or h_1, we obtain the admissible coordinate systems $(\lambda_{\gamma_4}, \lambda_{\beta_2})$ or $(\lambda_{\gamma_4}, \lambda_{\gamma_3})$. They have the same orientation. Now notice that for $l = 0$, see Fig. 10 a, there is a symmetry with respect to an interchange of the atoms $A_{\boxed{\gamma_4}}$ and $A_{\boxed{\gamma_1}}$. Therefore the statement carries over to the atom $A_{\boxed{\gamma_1}}$: the bases $(\lambda_{\gamma_1}, \lambda_{\beta_2})$, or $(\lambda_{\gamma_1}, \lambda_{\gamma_3})$ in Family (1) have the same orientation.

With these conventions, we scan through the admissible coordinate systems defined for Family (1) in the schemes (40), (41), and (43) to find that the bases

$$(\lambda_{\gamma_3}, \lambda_{\beta_1}), (\lambda_{\gamma_1}, \lambda_{\gamma_3})$$

have the same orientation as $(\lambda_{\gamma_1}, \lambda_{\alpha_1})$, while

$$(\lambda_{\beta_1}, -\lambda_{\gamma_5}), (\lambda_{\gamma_5}, \lambda_{\beta_1}), (\lambda_{\beta_1}, \lambda_{\beta_1} + \lambda_{\gamma_3}), (\lambda_{\beta_2}, \lambda_{\gamma_3}), (\lambda_{\gamma_3}, -\lambda_{\beta_2}), (\lambda_{\alpha_1}, \lambda_{\beta_1})$$

are oriented in the opposite sense.

It is not hard to check that the above conditions are sufficient to determine *uniquely* how the cycles λ_i related to Family (1) are located on the lattice Γ. Namely, λ_{γ_5} is homologous to λ_{α_1}, and λ_{β_2} to λ_{γ_5}. With the information on the orientations, we conclude that all three are the same. λ_{γ_3} has intersection indices 1 with λ_{γ_1} and λ_{β_2}; of the four possible locations on Γ, only one is allowed from the conventions on orientations. Finally, λ_{β_1} has intersection indices 1 with λ_{γ_3} and λ_{γ_5}. Taking into account the orientation, we find its location on Γ as shown in Fig. 13 a.

Family (2). This family participates in the bifurcations $A_{\boxed{\delta_1}}$, $B_{\boxed{\beta_1}}$, $B_{\boxed{\beta_3}}$, $A^*_{\boxed{\gamma_2}}$, $B_{\boxed{\gamma_6}}$. The singular points related to this family are U_1, U_2, M_2, e_1, e_2, h_2. The information on intersection indices is again obtained from the loop molecules in Table 4.

U_1: λ_{β_1} and λ_{γ_2} have intersection index 2.

U_2: λ_{β_1} and λ_{γ_6} as well as λ_{β_3} and λ_{γ_6} have intersection index 1.

M_2: λ_{δ_1} and λ_{γ_6} have intersection index 0, i.e., are homologous.

e_1: λ_{δ_1} and λ_{β_1} have intersection index 1.

e_2: λ_{δ_1} and λ_{β_3} have intersection index 1.

h_2: λ_{β_3} and λ_{γ_2} have intersection index 0, i.e., are homologous.

In this family, the orientation of bases

$$(\lambda_{\beta_1}, \lambda_{\gamma_6}), (\lambda_{\gamma_6}, -\lambda_{\beta_3}), (\lambda_{\gamma_2}, \tfrac{\lambda_{\beta_1}+\lambda_{\gamma_2}}{2})$$

coincides and is opposite to that of

$$(\lambda_{\delta_1}, \lambda_{\beta_1}), (\lambda_{\gamma_6}, \lambda_{\beta_1}).$$

The location of the cycles λ_i on the fundamental lattice of tori $T \in (2)$ is shown in Fig. 13 b.

Family (3). The bifurcations related to this family are $A_{\boxed{\alpha_2}}$, $C_2{}_{\boxed{\beta_2}}$, $B_{\boxed{\beta_3}}$, $A^*_{\boxed{\gamma_2}}$, $B_{\boxed{\gamma_5}}$. The singular points involved are U_1, U_2, U_3, e_2, h_1, h_2. Inspecting the corresponding loop molecules we get the following information.

U_1: λ_{β_2} and λ_{γ_2} have intersection index 1.

U_2: λ_{β_3} and λ_{γ_5} have intersection index 1.

U_3: λ_{α_2} and λ_{γ_5} have intersection index 0, i.e., are homologous.

e_2: λ_{α_2} and λ_{β_3} have intersection index 1.

h_1: λ_{β_2} and λ_{γ_5} have intersection index 0, i.e., are homologous.

h_2: λ_{β_3} and λ_{γ_2} have intersection index 0, i.e., are homologous.

The bases

$$(\lambda_{\gamma_5}, -\lambda_{\beta_3}), (\lambda_{\beta_2}, -\lambda_{\gamma_2})$$

have the same orientation while that of

$$(\lambda_{\beta_3}, -\lambda_{\gamma_5}), (\lambda_{\gamma_2}, -\lambda_{\beta_2}), (\lambda_{\alpha_2}, \lambda_{\beta_3})$$

is opposite. The result concerning the location of the five cycles involved is again unambiguous and presented in Fig. 13 c.

Family (4). The bifurcation related to this family are $C_2\boxed{\beta_2}$, $B\boxed{\gamma_3}$, $A\boxed{\gamma_4}$. The singular points to be considered are U_1, h_1, c_1:

U_1: λ_{β_2} and λ_{γ_3} have intersection index 1.

h_1: λ_{β_2} and λ_{γ_4} have intersection index 1.

c_1: λ_{γ_3} and λ_{γ_4} have intersection index 1.

The situation concerning orientations is rather simple. The basis

$$(\lambda_{\gamma_4}, \lambda_{\gamma_3})$$

has the opposite orientation from that of

$$(\lambda_{\beta_2}, \lambda_{\gamma_3}), (\lambda_{\gamma_3}, -\lambda_{\beta_2}).$$

The arrangement of the three λ_i on the lattice Γ is shown in Fig. 13 d.

Family (5). The bifurcations related to this family are $B\boxed{\beta_3}$, $B\boxed{\gamma_6}$, $A\boxed{\gamma_7}$, $A\boxed{\delta_2}$. The participating singular points are U_2, M_1, M_2, e_2, h_2, c_2.

U_2: λ_{β_3} and λ_{γ_6} have intersection index 1.

M_1: λ_{δ_2} and λ_{γ_7} have intersection index 1.

M_2: λ_{δ_2} and λ_{γ_6} have intersection index 0, i.e., are homologous.

e_2: λ_{δ_2} and λ_{β_3} have intersection index 1.

h_2: λ_{β_3} and λ_{γ_7} have intersection index 2.

c_2: λ_{δ_2} and λ_{β_3} have intersection index 1.

The orientation of the basis

$$(\lambda_{\beta_3}, \lambda_{\gamma_6})$$

is opposite to that of

$$(\lambda_{\delta_2}, \lambda_{\beta_3}), (\lambda_{\gamma_7}, \tfrac{\lambda_{\gamma_7}+\lambda_{\beta_3}}{2}).$$

The four cycles λ_i involved are located on the lattice Γ of Family (5) as shown in Fig. 13 e.

4.4 Gluing matrices and numerical marks

It is now a matter of simple bookkeeping to assemble the gluing matrices for all edges in the ten possible types of isoenergy molecules.

Consider, for example, the molecule denoted by D in [11]:

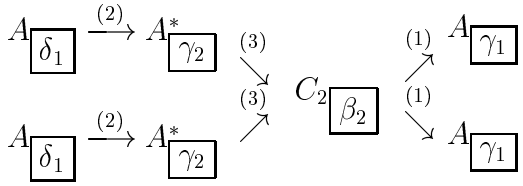

(48)

Each edge represents a Family (n) of tori and connects two bifurcations i and j. In the first step, check out from the listings in (40), (41), (43), which admissible coordinate system applies to the bifurcations i and j in Family (n). In Family (1) this is $(\lambda_{\gamma_1}, \lambda_{\gamma_3})$ for γ_1 and $(\lambda_{\beta_2}, \lambda_{\gamma_3})$ for β_2. The second step is to look up Fig. 13 for the lattice Γ of Family (n). In Fig. 13 a we see that $\lambda_{\gamma_1} = \lambda_{\gamma_3} - \lambda_{\beta_2}$. This gives immediately

$$\begin{pmatrix} \lambda_{\gamma_1} \\ \lambda_{\gamma_3} \end{pmatrix} = \mathbf{C} \begin{pmatrix} \lambda_{\beta_2} \\ \lambda_{\gamma_3} \end{pmatrix} = \begin{pmatrix} -1 & 1 \\ 0 & 1 \end{pmatrix} \begin{pmatrix} \lambda_{\beta_2} \\ \lambda_{\gamma_3} \end{pmatrix} \tag{49}$$

for the two edges at the right end of (48). In the same way we obtain

$$\begin{pmatrix} \lambda_{\beta_2} \\ -\lambda_{\gamma_2} \end{pmatrix} = \mathbf{C} \begin{pmatrix} \lambda_{\gamma_2} \\ -\lambda_{\beta_2} \end{pmatrix} = \begin{pmatrix} 0 & -1 \\ -1 & 0 \end{pmatrix} \begin{pmatrix} \lambda_{\gamma_2} \\ -\lambda_{\beta_2} \end{pmatrix} \tag{50}$$

for the edges involving Family (3), and

$$\begin{pmatrix} \lambda_{\gamma_2} \\ \frac{\lambda_{\beta_1}+\lambda_{\gamma_2}}{2} \end{pmatrix} = \mathbf{C} \begin{pmatrix} \lambda_{\delta_1} \\ \lambda_{\beta_1} \end{pmatrix} = \begin{pmatrix} -2 & 1 \\ -1 & 1 \end{pmatrix} \begin{pmatrix} \lambda_{\delta_1} \\ \lambda_{\beta_1} \end{pmatrix} \tag{51}$$

for the edges involving Family (2).

Proceeding in this manner with all molecules in Table 3, we obtain the gluing matrices for the ten types of Liouville foliations on isoenergy surfaces, see Table 5.

The collection of gluing matrices of a molecule has been called its *redundant frame* in [7, 6]. "Redundant" means that there is more information in the matrices than we need to completely determine the topology of the foliation; this reflects the fact that admissible coordinate systems and, consequently, gluing matrices are not uniquely defined. In [7, 6] we suggest a procedure to reduce the information and make it unambiguous. Instead of gluing matrices we consider certain numerical marks (r, ε, n) which satisfy the following natural properties:

1) they are calculated uniquely from the gluing matrices,

2) they do not change under a transformation of admissible coordinate systems,

3) the gluing matrices can be reconstructed from these marks uniquely up to admissible coordinate system transformations.

Thus, replacing the gluing matrices with these marks we do not lose any important information but reduce it to its uniquely defined essence. The result is given in Table 3.

This procedure completes the proof of the theorem. The definitions and formal rules for calculation of (r, ε, n) can be found in [7, 6]. We omit these calculations here. The result is exactly the statement of the Theorem.

References

[1] G. G. Appelrot. Not entirely symmetrical heavy gyroscopes (in Russian). In *Rigid Body Motion About a Fixed Point, Collection of papers in memory of S. V. Kovalevskaya*, pages 61–155. Acad. Sci. USSR, Dept. of Technical Sciences, Moscow, Leningrad, 1940.

[2] M. Audin. *Spinning Tops.* Cambridge University Press, Cambridge, 1996.

[3] A. I. Bobenko, A. G. Reyman, and M. A. Semenov Tian Shansky. The Kowalewski top 99 years later: A Lax pair, generalizations and explicit solutions. *Commun. Math. Phys.*, 122:321–354, 1989.

[4] A. V. Bolsinov. Methods of calculation of the Fomenko-Zieschang invariant. In A. T. Fomenko, editor, *Topological Classification of Integrable Systems*, pages 147–183, Providence, RI, 1991. American Mathematical Society.

[5] A. V. Bolsinov and A. T. Fomenko. *Introduction to the Topology of Integrable Hamiltonian Systems.* Nauka, Moscow, 1997.

[6] A. V. Bolsinov and A. T. Fomenko. *Integrable Hamiltonian Systems. Geometry, Topology, Classification. Vol. I and II.* Udmurt. Univ. Publ., Izhevsk, 1999. (Russian).

[7] A. V. Bolsinov, S. V. Matveev, and A. T. Fomenko. Topological classification of integrable Hamiltonian systems with two degrees of freedom. List of systems of low complexity. *Uspekhi Matem. Nauk*, 45(2):49–77, 1990.

[8] R. Cooke. *The Mathematics of Sonya Kovalevskaya.* Springer, Berlin, Heidelberg, New York, 1984.

[9] R. H. Cushman and L. M. Bates. *Global Aspects of Classical Integrable Systems.* Birkhäuser, Basel, Boston, Berlin, 1997.

[10] H. R. Dullin. *Die Energieflächen des Kowalewskaja-Kreisels.* Mainz Verlag, Aachen, 1994. Dissertation Univ. Bremen, in German.

[11] H. R. Dullin, M. Juhnke, and P. H. Richter. Action integrals and energy surfaces of the Kovalevskaya top. *Bifurcation and Chaos*, 4(6):1535–1562, 1994.

[12] H. R. Dullin, P. H. Richter, and A. P. Veselov. Action variables of the Kovalevskaya top. *Regular and Chaotic Dynamics*, 3(3):18–31, 1998.

[13] A. T. Fomenko. Topological classification of all integrable Hamiltonian differential equations of general type with two degrees of freedom. In T. Ratiu, editor, *The Geometry of Hamiltonian Systems*, pages 131–339, New York, 1991. Springer.

[14] V. V. Kalashnikov. Typical integrable Hamiltonian systems on a four-dimensional symplectic manifold. *Izvestiya RAN, seriya matem.*, 62(2):49–74, 1998.

[15] M. P. Kharlamov. Bifurcation of common levels of first integrals of the Kovalevskaya problem. *Prikl. Matem. Mekhan.*, 47(6):737–743, 1983.

[16] M. P. Kharlamov. *Topological Analysis of Integrable Problems in Rigid Body Dynamics*. Leningrad Univ. Publ., Leningrad, 1988.

[17] F. Klein and A. Sommerfeld. *Über die Theorie des Kreisels*. Teubner, Leipzig, 1910.

[18] F. Kötter. Sur le cas traité par Mme Kowalevski de rotation d'un corps solide autour d'un point fixe. *Acta Math.*, 17:209–264, 1893.

[19] S. Kowalevski. Sur le problème de la rotation d'un corps solide d'un point fixe. *Acta Math.*, 12:177–232, 1889.

[20] S. Kowalevski. Sur une propriété du système d'équations différentielles qui définit la rotation d'un corps solide d'un point fixe. *Acta Math.*, 14:81–93, 1889.

[21] L. M. Lerman and Ya. L. Umanskii. The classification of four-dimensional integrable systems and the Poisson action of R^2 in extended neighborhoods of simple singular points. I. *Matem. Sbornik*, 183(12):141–176, 1992.

[22] V. S. Matveev. Integrable Hamiltonian systems with two degrees of freedom. Topological structure of saturated neighborhoods of saddle-saddle and focus-focus types. *Matem. Sbornik*, 187(4):29–58, 1996.

[23] A. A. Oshemkov. Fomenko invariants for the main integrable cases of the rigid body motion equations. In A. T. Fomenko, editor, *Topological Classification of Integrable Systems*, pages 67–146, Providence, RI, 1991. American Mathematical Society.

[24] A. A. Oshemkov. The calculation of Fomenko's invariants for the main integrable cases in rigid body dynamics. In *Trudy seminara po. vekt. i tenz. analizu*, volume 25/2, pages 23–109. Moscow State Univ. Publ., Moscow, 1993.

[25] P. H. Richter, H. R. Dullin, and A. Wittek. Kovalevskaya Top. *Publ. Wiss. Film., Sekt. Techn. Wiss./Naturwiss.*, 13:33–96, 1997. Film C1961, Inst. Wiss. Film (IWF), Göttingen.

[26] N. E. Zhukovsky. Geometric interpretation of the case considered by Kovalevskaya of the motion of a heavy rigid body about a fixed point. *Mat. Sbornik*, 19:45–93, 1896.

Figure 1:

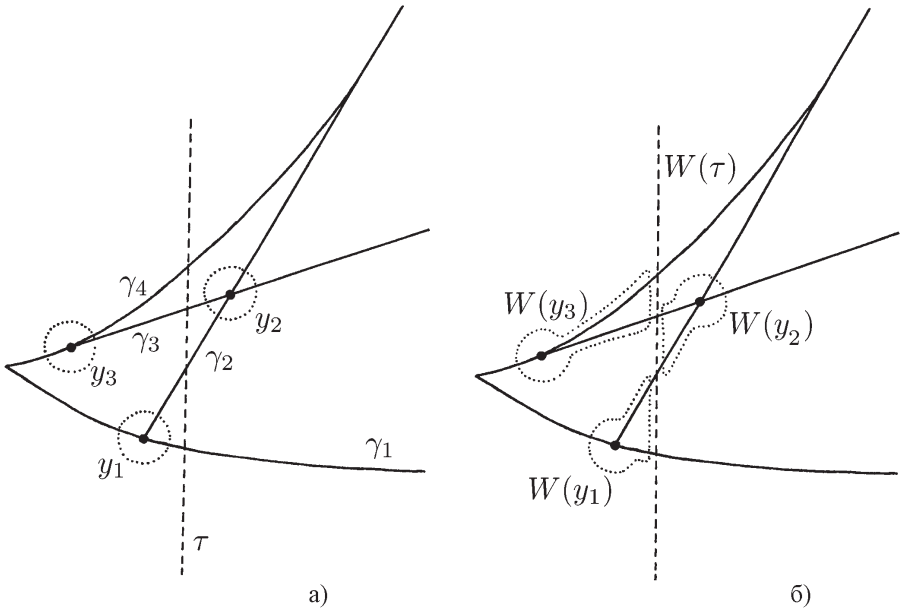

а) б)

Figure 2:

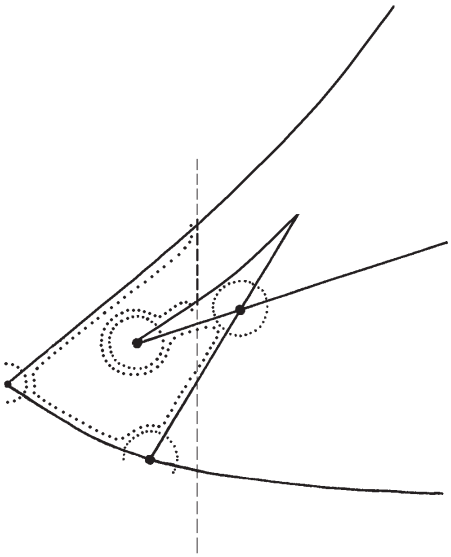

Figure 3:

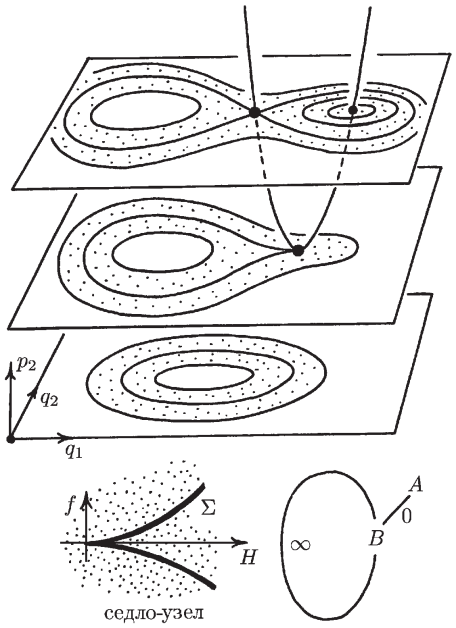

Figure 4:

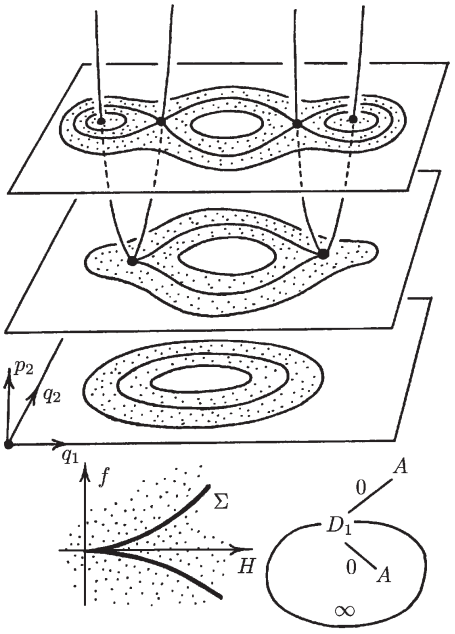

Figure 5:

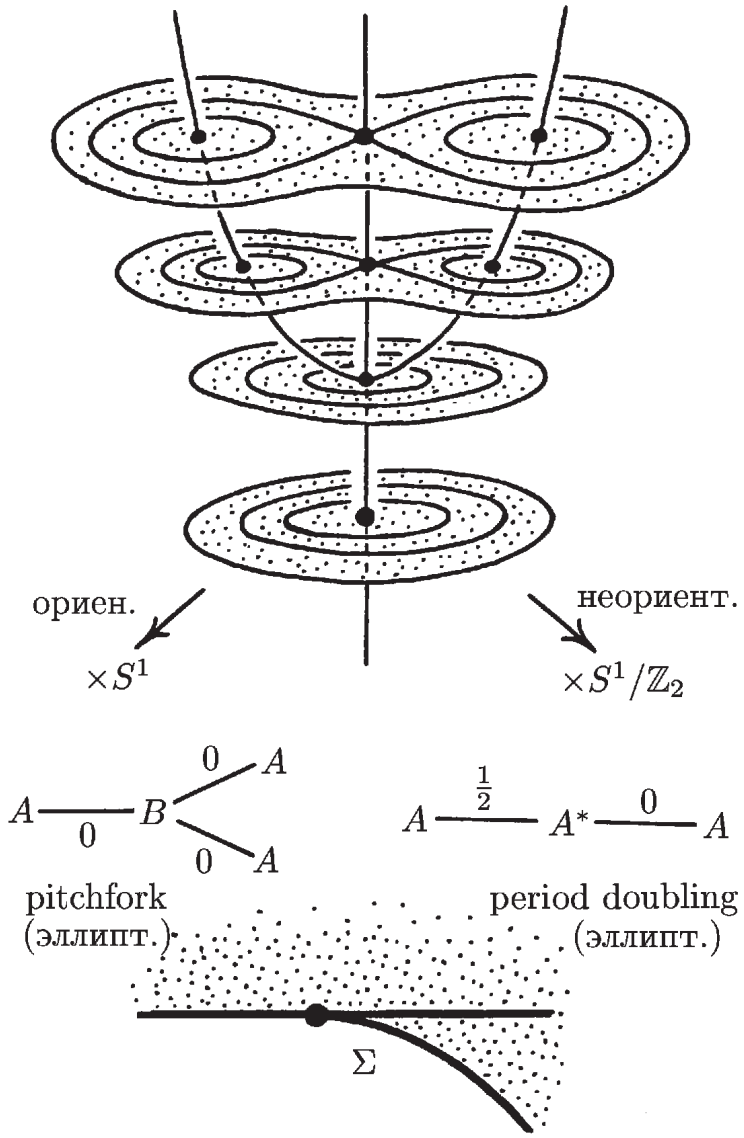
ориен.
неориент.
$\times S^1$
$\times S^1/\mathbb{Z}_2$
A — 0 — B — 0 — A
B — 0 — A
A — $\frac{1}{2}$ — A^* — 0 — A
pitchfork
(эллипт.)
period doubling
(эллипт.)
Σ

Figure 6:

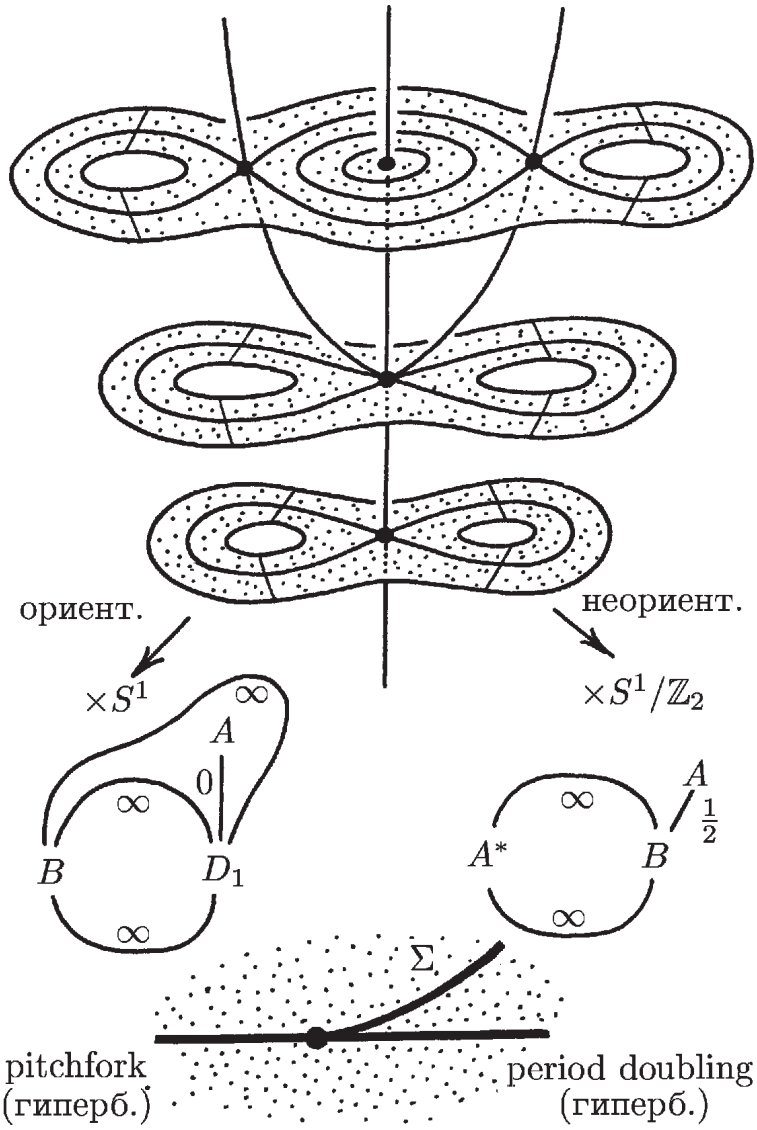
ориент.
неориент.
$\times S^1$
$\times S^1/\mathbb{Z}_2$
∞
A
0
∞
B
D_1
∞
∞
A
$\frac{1}{2}$
A^*
B
∞
Σ
pitchfork
(гиперб.)
period doubling
(гиперб.)

Figure 7:

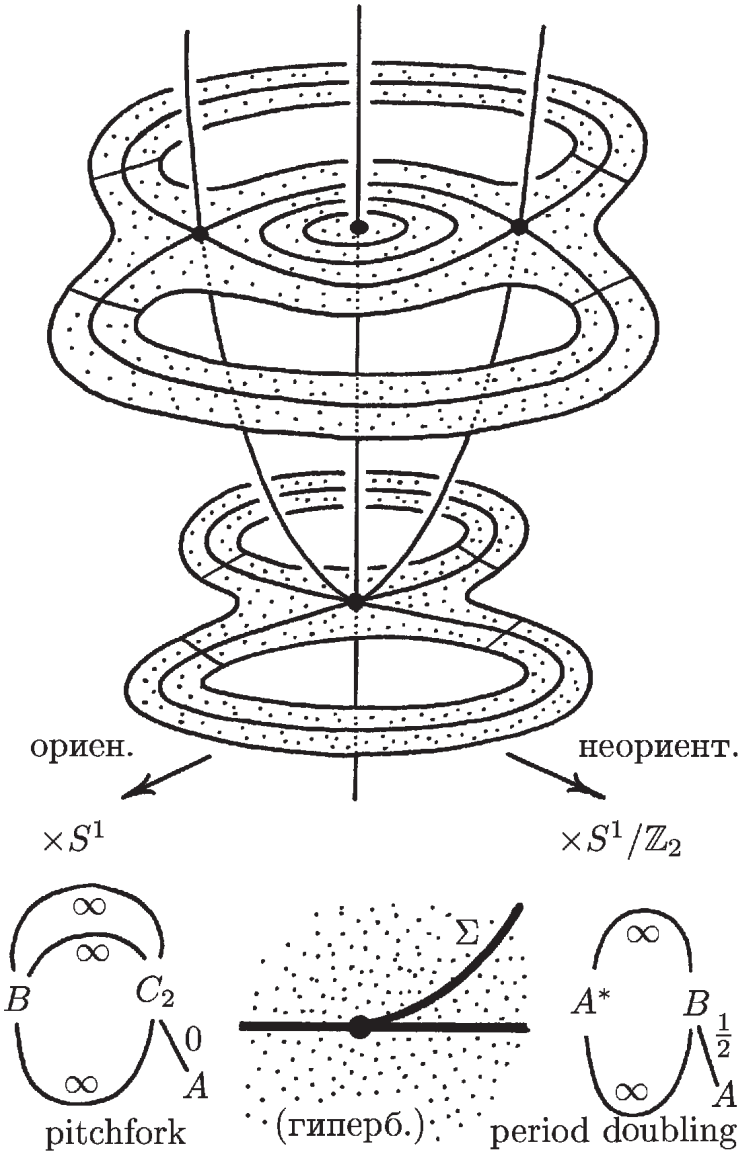
ориен.
неориент.
$\times S^1$
$\times S^1/\mathbb{Z}_2$
∞
∞
B
C_2
0
∞
A
pitchfork
Σ
(гиперб.)
∞
A^*
B
$\frac{1}{2}$
∞
A
period doubling

Figure 8:

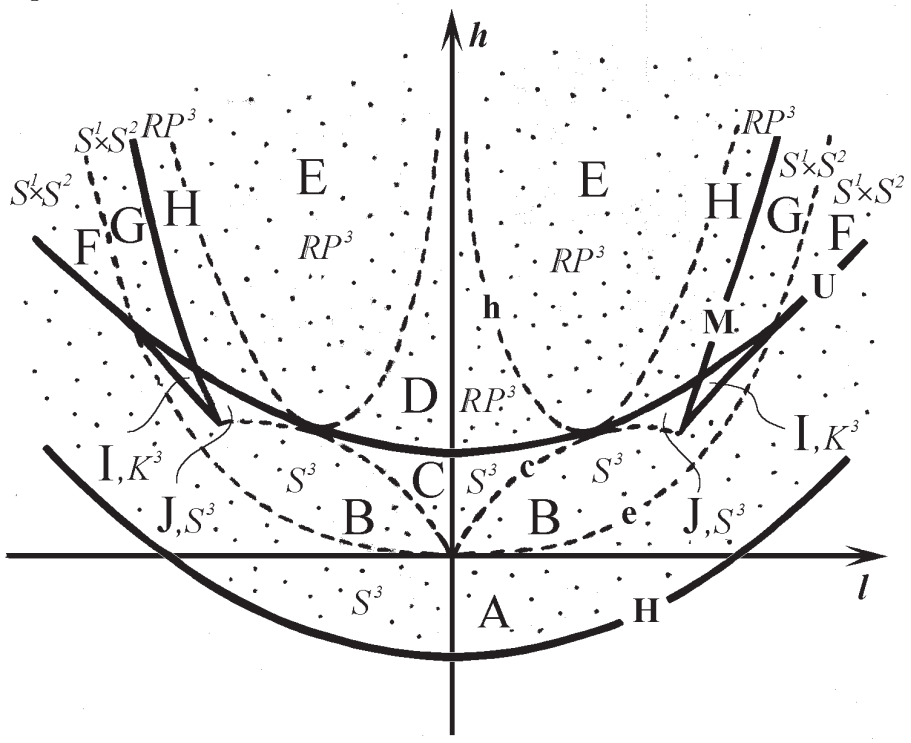

Figure 9:

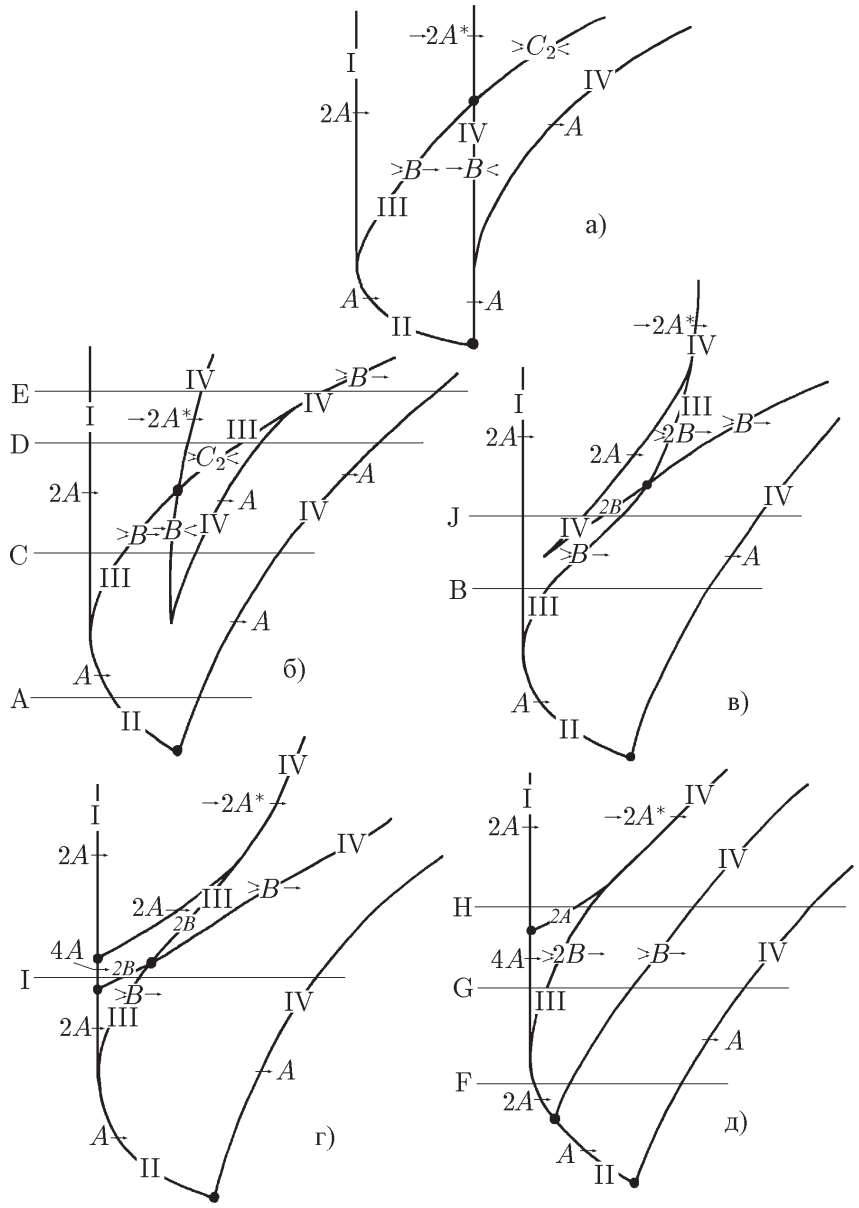
I
2A
→2A*←
>C2<
IV
A
IV
>B→ →B<
III
A
A
II
а)
E
D
C
A
I
2A
IV
→2A*←
III
>C2<
IV
>B→
A
A
>B→B<IV
IV
A
III
A
A
II
б)
I
2A
IV
→2A*←
III
2A
>2B→
>B→
J
B
2B
IV
IV
>B→
A
III
A
II
в)
I
2A
IV
→2A*←
IV
2A
III
2B
>B→
4A
2B
I
>B→
2A
III
IV
A
A
II
г)
I
2A
IV
→2A*←
IV
H
2A
4A
>2B→
>B→
IV
G
III
A
F
2A
A
II
д)

Figure 10:

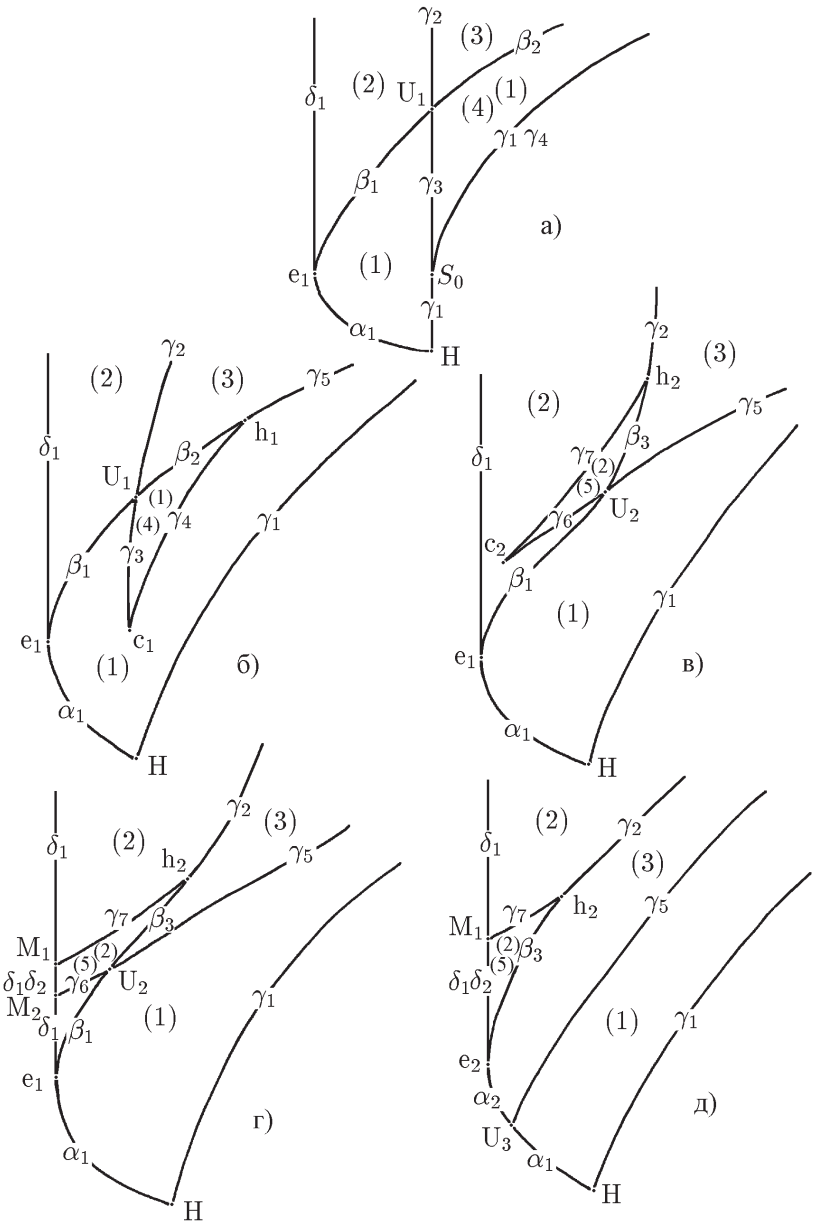
а)
б)
в)
г)
д)
H
S_0
U_1
U_2
U_3
h_1
h_2
c_1
c_2
e_1
e_2
M_1
M_2
δ_1
$\delta_1\delta_2$
α_1
α_2
β_1
β_2
β_3
γ_1
γ_2
γ_3
γ_4
γ_5
γ_6
γ_7
(1)
(2)
(3)
(4)
(5)

Figure 11a:

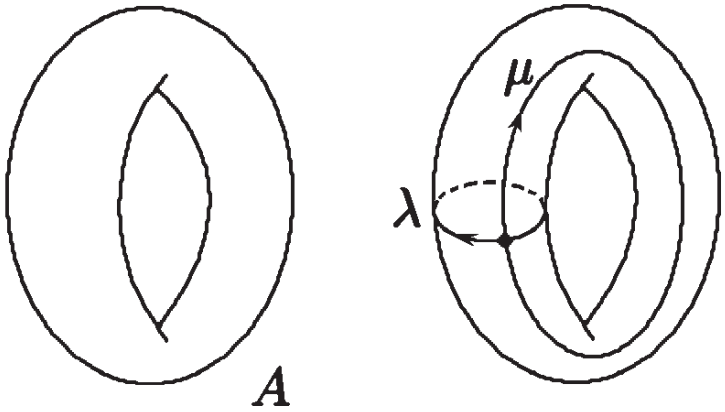

Figure 11b:

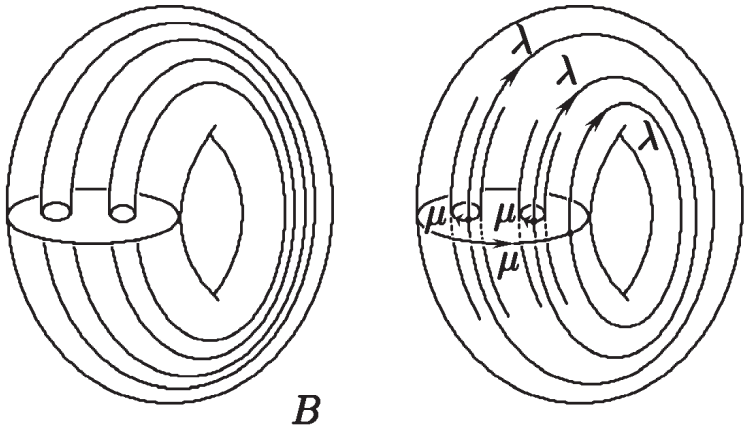

Figure 11 c:

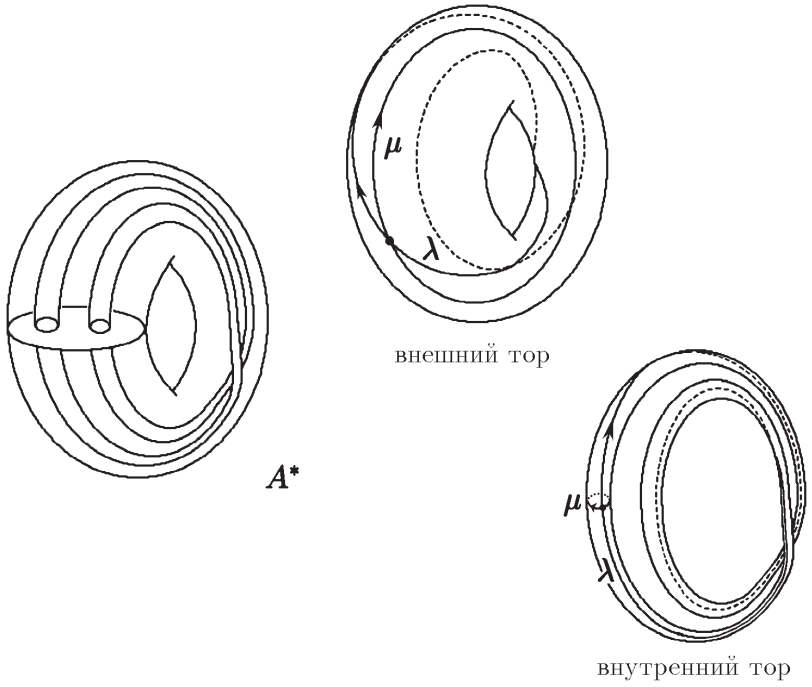

Figure 11 d:

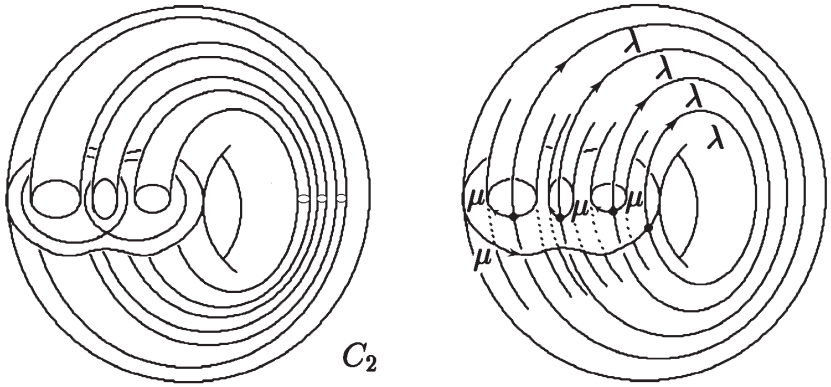

Figure 12:

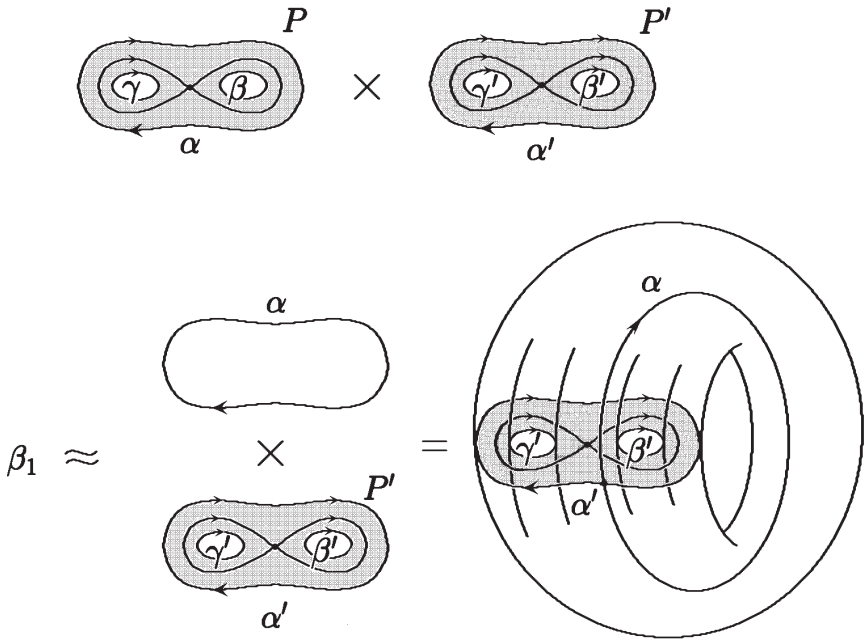

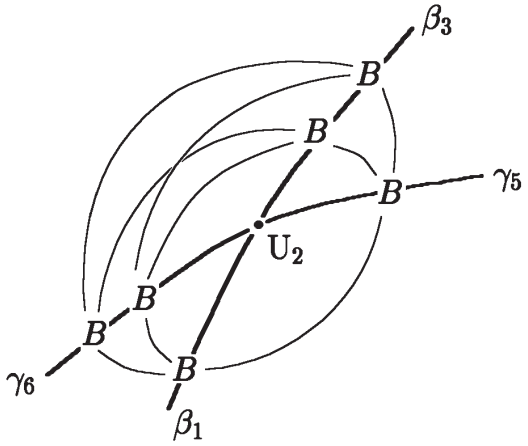

Figure 13:

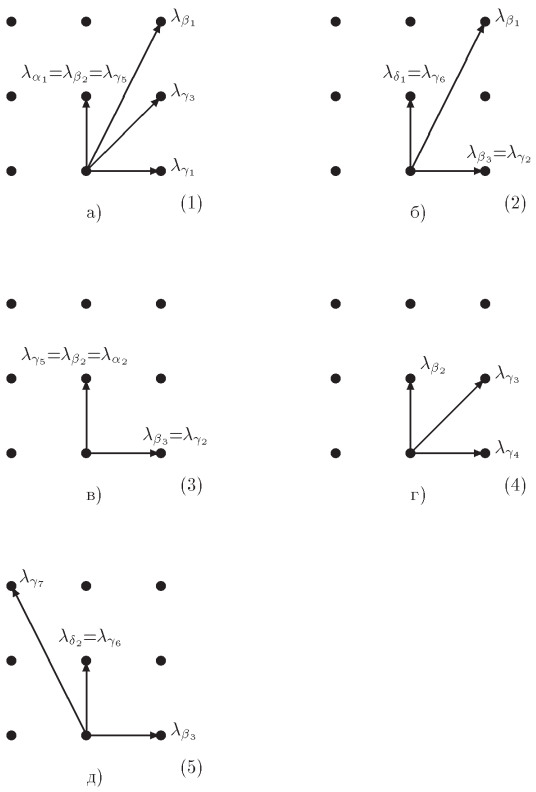

Рис. 14

1

Table 1. Loop molecules for nondegenerate equilibria

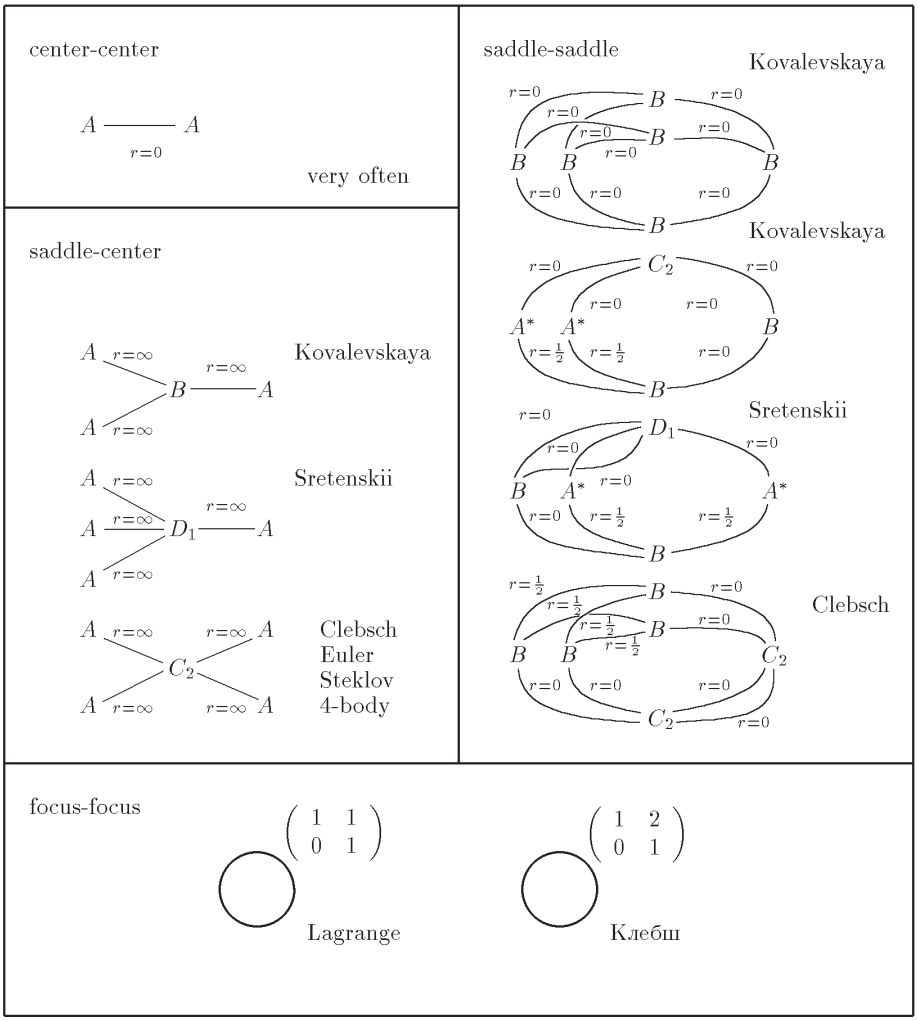

Table 2. Circle molecules for degenerate one-dimensional orbits

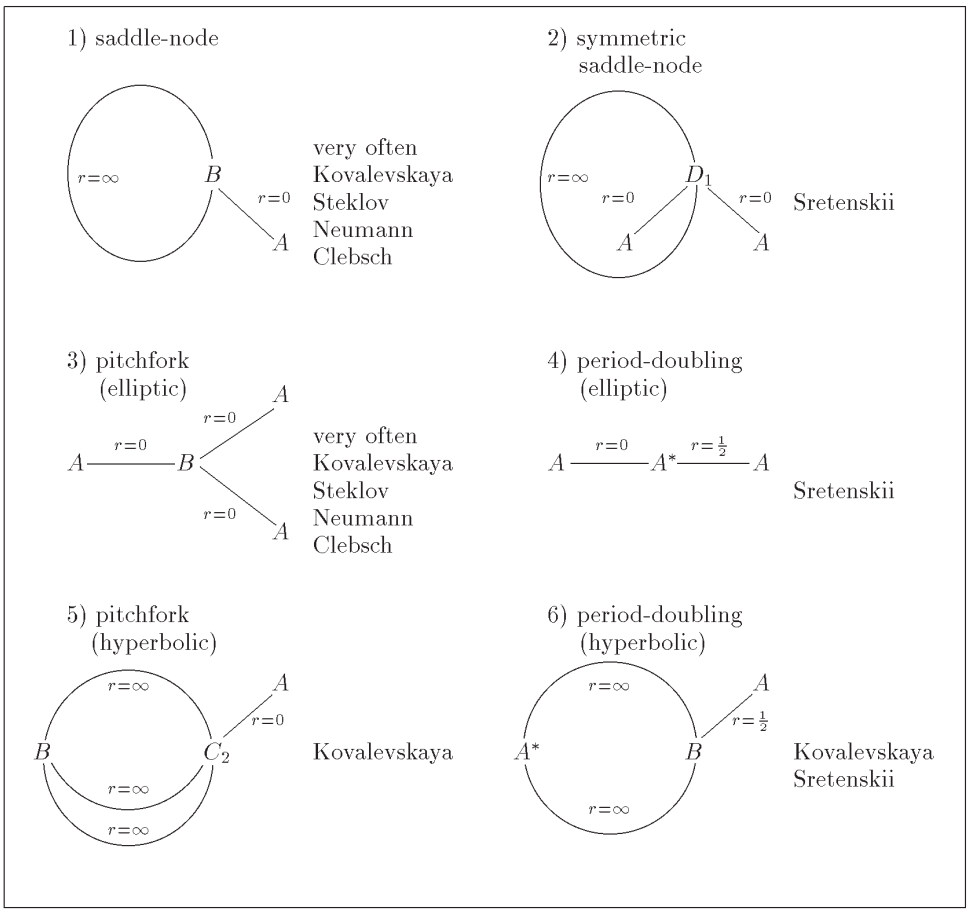

Table 3. Marked molecules for the Kovalevskaya top

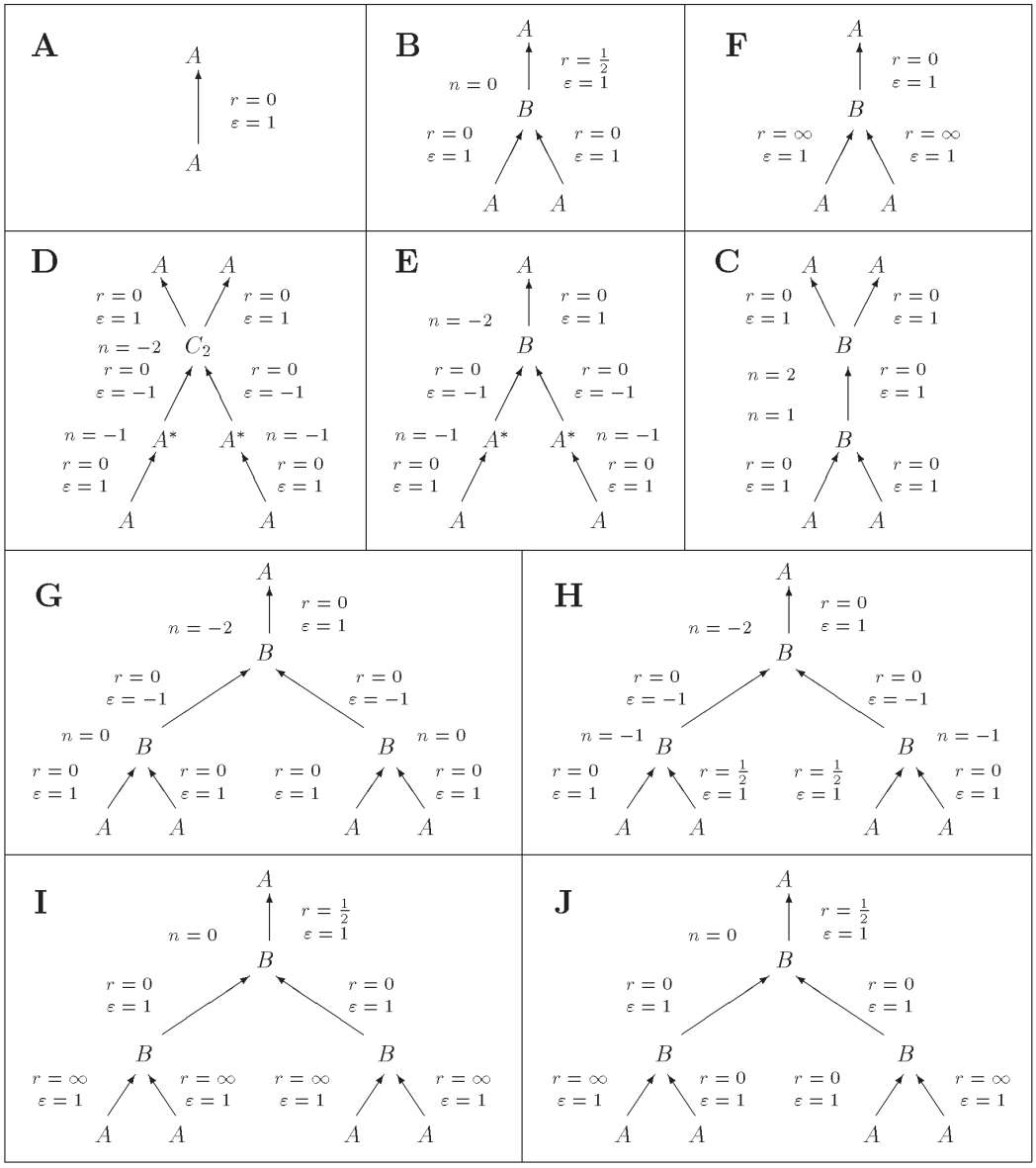

Table 4. Loop molecules for the Kovalevskaya top

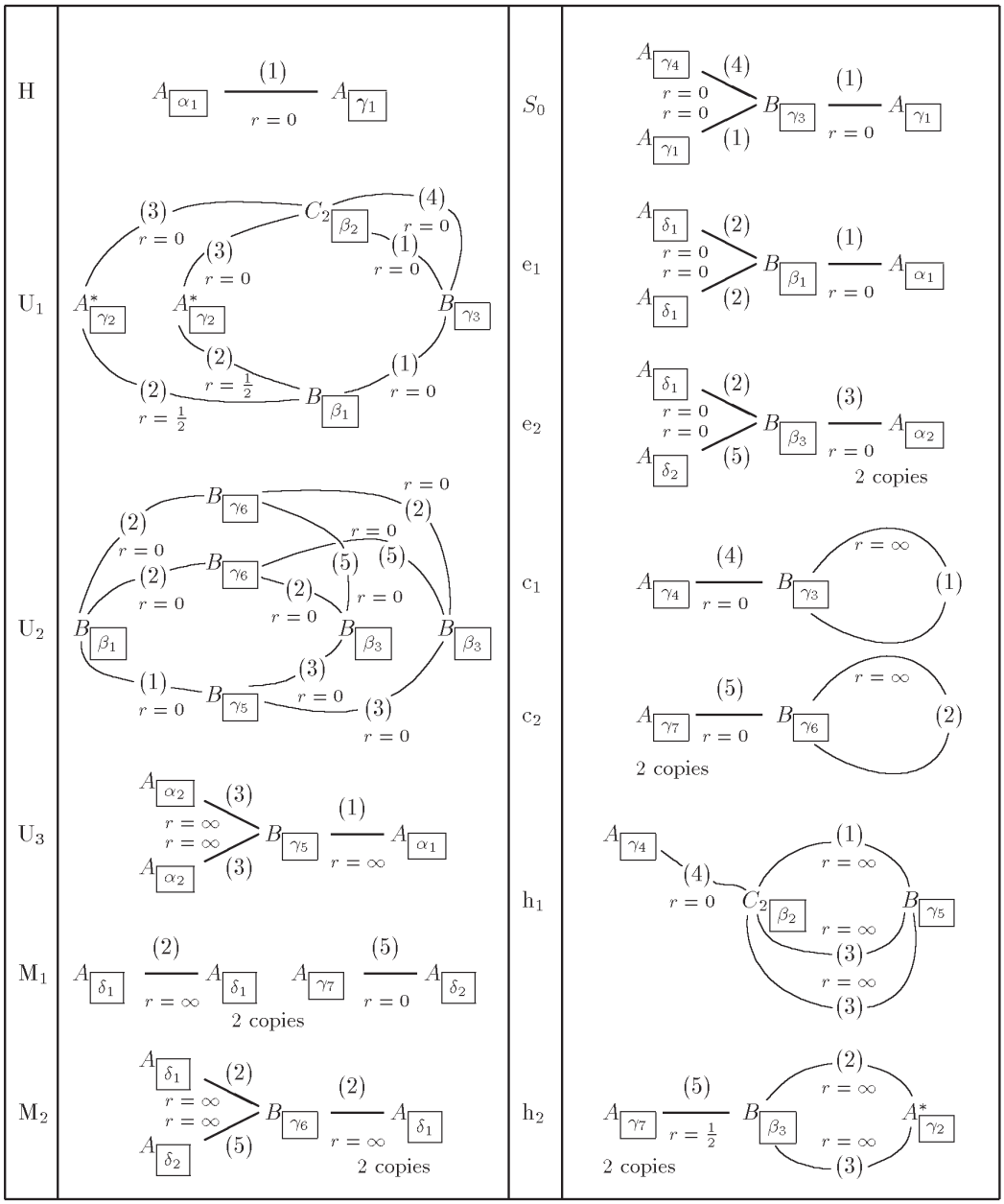

Table 5. Gluing matrices